EVALUATING THE PERFORMANCE OF NSSLTDA and NFTDA TORNADO DETECTION ALGORITHMS

Nilson Eduardo Torres Barreto

Universidad Industrial de Santander
Faculty of Physical and mechanical Engineering
School of Electrical and Computer Engineering
Bucaramanga
2009

EVALUATING THE PERFORMANCE OF NSSLTDA and NFTDA TORNADO DETECTION ALGORITHMS

Nilson Eduardo Torres Barreto

Thesis work pursuing bachelor degree in science, BSC

Dr. Tian-Yuo Yu, Director, Dr. Valliappa Lakshamanan, Advisor, Dr. Gregory Stumpf, Advisor, Dr. Yadong wang, Advisor

Universidad Industrial de Santander
Faculty of Physical and mechanical Engineering
School of Electrical and Computer Engineering
Bucaramanga
2009

This achievement is dedicated primary to God who has given me the strength to conclude this project, to my parents, who have always believed and supported me. To friends and family members, none of this could be done without their love and advisory.

ACKNOWLEDGMENTS

The author expresses his acknowledgments to:

Dr. Tian-You Yu for his continuous guidance, orientation, support, his patience and his helpful advises. His students in the ARRC (Atmospheric Research Radar Center) were very helpful as well.

Dr. Yadong Wang, who was the developer of the base NFTDA algorithm. Without his astonishing work and his continuous dedication to the algorithm and to this project, none of this could be done in time.

Dr. Valliappa Lakshamanan for his dedication, commitment, his persistency and mostly the love he had for the topic which was successfully transmitted to me. His support on the WDSSII as a developer was invaluable.

Dr. Greg Stumpf, who provided crucial data for the algorithm and assistance, which helped on the development of the thesis. I appreciate the effort that the WATADS and the WDTB teams injected to gather up all this information and organize it in such a consistent form.

To my fellow team mates in the NOAA and the ARRC who gave me important information and support when I most needed it.

CONTENTS

TABLE LIST

FIGURE LIST

TITLE: EVALUATING THE PERFORMANCE OF NSSLTDA and NFTDA TORNADO DETECTION ALGORITHMS*

AUTHOR: Nilson Eduardo Torres Barreto**

KEY WORDS: Tornado, Radar, Weather, Storm, Mesocyclone, Algorithm, Transmitter, Receiver,

CONTENTS: Tornado vortices observed by Doppler radars are often related with high azimuthal shear and Doppler spectra that are wide and flattened. The current operational tornado detection algorithm (TDA) primarily searches for shear signatures that are larger than the predefined thresholds. In this work, a tornado detection procedure based on a fuzzy logic system is tested to integrate tornadic signatures in both the velocity and spectral domains. A novel feature of the system is that it is further enhanced by a neural network to refine the membership functions through a feedback training process. The hybrid approach herein, termed the neuro–fuzzy tornado detection algorithm (NFTDA), is initially verified using simulations and is subsequently tested on real data. These simulations are ingested in software developed by the author which contrasts both TDA and NFTDA algorithms. The results demonstrate not only that NFTDA can detect tornadoes even when the shear signatures are degraded significantly so that they would create difficulties for typical vortex detection schemes, but that NFTDA is overall more accurate in all sorts of scenarios. The performance of the NFTDA and TDA is assessed with level I time series data collected by the NEXRAD, a network of 158 operational radars known as: Weather Surveillance Radar-1988 Doppler (WSR-88D) operated by several agencies, including the National Severe Storms Laboratory (NSSL) and National Oceanographic Atmospheric Administration (NOAA), during several tornado outbreaks occurred along the United States. Additional Ground Truth Data was collected by the WDTB and the WATADS team in order to verify all sorts of digital data.

---

* Proyecto de Grado

** Facultad: Facultad de Ingenierías Físico Mecánicas. Escuela: Ingeniería Eléctrica Electrónica y Telecomunicaciones. Director: Dr.Tian-You Yu.

TÍTULO: EVALUACIÓN DE DESEMPEÑO DE LOS ALGORITMOS DE DETECCION DE TORNADOS NSSLTDA Y NFTDA *

AUTOR: Nilson Eduardo Torres Barreto**

PALABRAS CLAVE: Tornado, Radar, Tiempo, Tormenta, Meso-ciclón, Algoritmo, transmisor, receptor,

CONTENIDO: Vortices de Tornado observados por radares Doppler a menudo están relacionadas con una alta cizalladura de Reflectividad en azimut y una respuesta en frecuencia (espectro Doppler) ancha y aplanada. El funcionamiento actual del algoritmo de detección de tornados (TDA) en primer lugar busca indicios de cizalladuras que son más grandes que unos umbrales predefinidos. En este trabajo, un procedimiento de detección de tornados basado en un sistema de lógica difusa se prueba para integrar indicios tornadicos tanto en la velocidad como en el dominio espectral. Una nueva característica del sistema es que es reforzado por una red neuronal para perfeccionar la composición de funciones propias de dicha red, a través de un proceso de entrenamiento mediante retroalimentación. Este enfoque híbrido, se denomino “NEURO-FUZZY TORNADO DETECTION ALGORITHM” (NFTDA), e inicialmente se verificó mediante simulaciones y posteriormente se probó en datos reales. Estas simulaciones son ingeridas en un software desarrollado por el autor, que contrasta tanto a TDA como a NFTDA. Los resultados demuestran que el algoritmo NFTDA no solo se comporta mejor en general, sino también en casos en los cuales el otro algoritmo tendría dificultades al detectar dichos fenómenos, como por ejemplo eventos tornadicos a corta y a larga distancia del radar con el cual se hace la medición. El desempeño de los algoritmos TDA y NFTDA se evalúan con un nivel I de series temporales de datos recogidos por la NEXRAD, una red operativa de 158 radares conocido como: “Weather Survailance Radar 1988 Doppler” (WSR-88D), operados por varios organismos, entre ellos el “National Severe Storm Laboratory” (NSSL) “National Oceanographic Atmospheric Administration” (NOAA), durante varios tornados que se produjeron largo de los Estados Unidos. Datos de campo fueron recopilados por la WDTB y la WATADS a fin de verificar todo tipo de informacion recolectada digitalmente.

---

* Proyecto de Grado

** Facultad: Facultad de Ingenierías Físico Mecánicas. Escuela: Ingeniería Eléctrica Electrónica y Telecomunicaciones. Director: Dr.Tian-You Yu.

INTRODUCTION

The first use of radio waves to detect a large metallic body at a large distance was when Christian Hulsmeyer demonstrated the feasibility of detecting the presence of a ship in dense fog, but not its distance. It was before the Second World War that developments by the Americans, Germans, French and mostly the British (whose first use was as a defense against aircraft attack), lead to the first radars (Radio Detection and Ranging).

Although Radars have many applications in military, aviation and various researches, one of the most important is the aid of weather forecasting. This has gained importance over the years, due to the many disasters it has carried. Some of the agencies that have been involved in the research and development of new techniques and technologies which have been widely used to reduce the impact of severe events over the population are: The NOAA (National Oceanographic and Atmospheric Administration), NWS (National Weather Service) which is one of the six scientific agencies of the NOAA, The National Severe Storms Laboratory (NSSL), which partners with NOAA, the Radar Operation Center (ROC), finally the warning decision Training Branch (WDTB) (**See figure 1**).

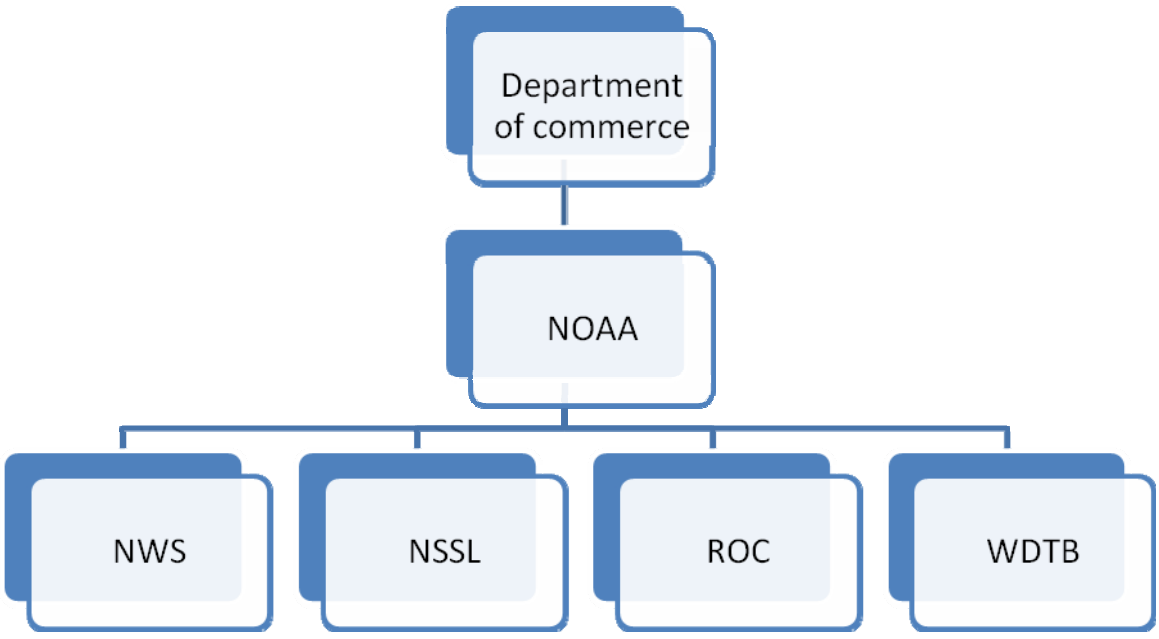

Figure 1. Different Departments on Radar Field

To understand the importance of a severe weather socially and economically, we first introduce table 1.
Brooks et al. (2000) made an interesting report about the cost of a damage left by a tornado. He analyzed the thirty most costly tornadoes from a database ranging from 1890 to 1999. Results shown are devastating, according to Brooks, they estimated that the costliest tornado was on the 3 may 1999 with an adjusted (adjusted for inflation) $963 million dollars in damage (constant 1997 dollars).

Rank	Date	Locaion	Raw (Million USD)	Adjusted (Million USD)
1	3 may 1999	Oklahoma city, OK	1000	963
2	10 apr 1979	Wichita Falls, TX	400	884
3	6 may 1975	Omaha, NE	250	745
4	11 may 1970	Lubbock, TX	135	558
5	8 jun 1966	Topeka, KS	100	494
6	3 oct 1979	Windsor Locks, CT	200	442
7	27 may 1896	St. Louis, MO-E. St. Louis, IL	12	380
8	3 apr 1974	Xenia, OH	100	325
9	31 mar 1973	Conyers, GA	89	321
10	9 jun 1953	Worcester, MA	52	311
11	3 jun 1980	Grand Island, NE	140	273
T12	11 may 1953	Waco, TX	41	246
T12	3 dec 1978	Bossier City, LA	100	246
14	20 may 1957	Ruskin Heights, MO	40	228
T15	29 sept 1927	St. Louis, MO	22	203
T15	28 aug 1990	Plainfield, IL	165	203
17	11 apr 1965	Branch County, MI	35	178
18	24 mar 1975	Atlanta, GA	56	167
19	29 may 1982	Marion, IL	100	166
20	3 apr 1974	Monticello, IN	50	163
T21	18 mar 1925	Tri-State (MO-IL-IN)	16	151
T21	6 apr 1936	Gainsville, GA	13	151
23	5 dec 1953	Vicksburg, MS	25	150
24	31 may 1985	Niles, OH-Wheatland, PA	100	149
25	4 apr 1966	Polk County, FL	30	148
26	21 apr 1967	Oak lawn, IL	30	144
T27	23 apr 1968	Falmouth, KY-Ripley, OH	30	138
T27	15 may 1968	Charles City, IA	30	138
29	23 jun 1944	Southwestern PA	15	137
30	15 nov 1989	Huntsville, AL	100	129

Table 1. Tornado damage cost estimate

Location means the most devastated region, Raw, is the raw damage amount in Million dollars and adjusted is the amount adjusted to 1997 Million dollars. The letter T indicates a tie. Brooks et al. (2000).
From only these 30 tornados, we can obtain an adjusted estimate of 8,931 million dollars total.

On table 2 we can see the amount of damages in dollars and the number of fatalities and injuries related to tornadic events over the last 6 years. This information is obtained from the annual storm data publication from the NCDC (National Climatic Data Center).

YEAR	INJURIES	FATALITIES	TOTAL DAMAGE COST (Million dollars)
2005	537	38	503.9
2004	396	35	549.2
2003	1087	54	1,281.5
2002	968	55	802.1
2001	743	40	637.5
TOTAL	3731	222	2,972.1

Table 2. Side effects of tornadic events over several years. source NCDC: Storm data publications

This data implies that the number of injuries and fatalities has been decreasing thanks to the increase in research and development, as seen in figures 2, 3 and 4.

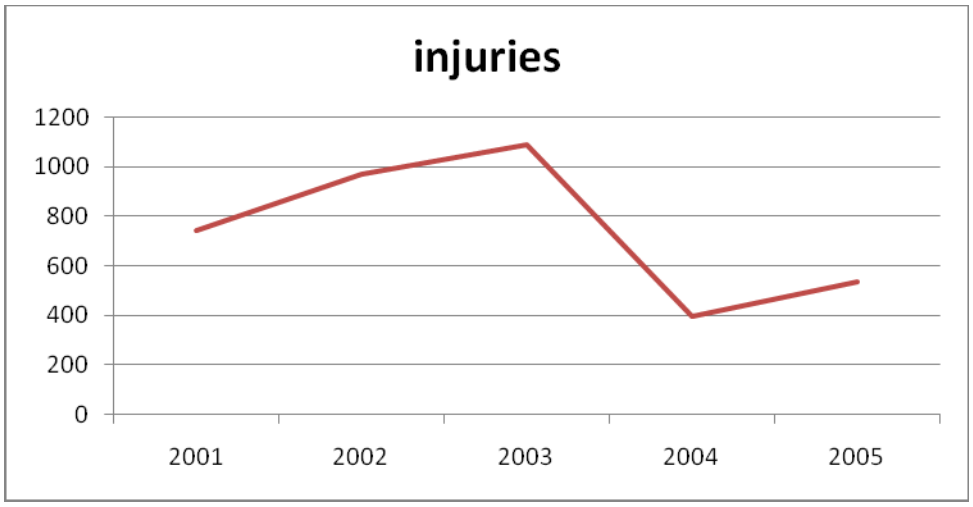

Figure 2. Number of injuries Vs. years according to NCDC storm data publications

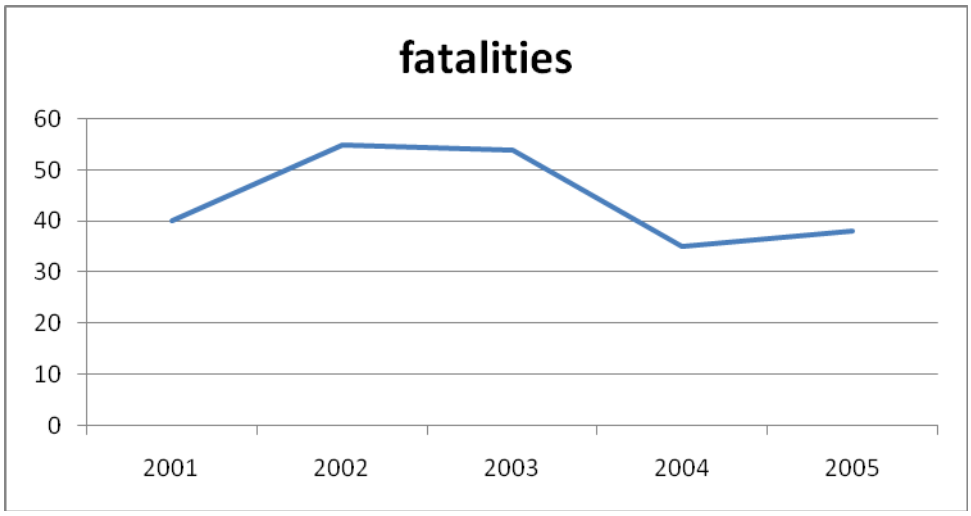

Figure 3. Number of fatalities vs. years according to the NCDC storm data publications

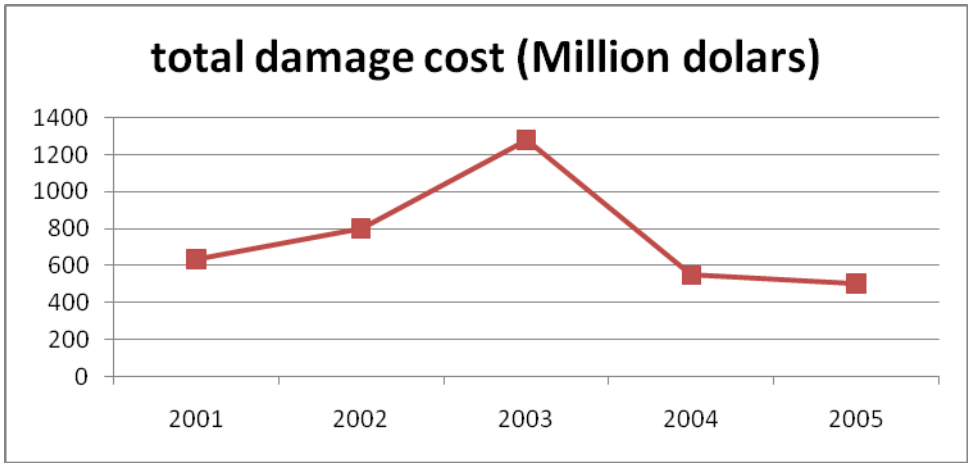

Figure 4. Total damage cost in million dollars vs years according to NCDC storm data publications

On figure 5, we present how the tornados affect the population demographically. This indicates that the central region has more propensity of being struck by a tornado than other regions of the United States. This information was provided by the Oklahoma Climatological survey and from the university of Oklahoma police department.

Tornado warnings have improved significantly and the number of tornado casualties has decreased by nearly half since a network of Doppler weather radars were installed nationwide by the National Oceanic and Atmospheric Administration's National Weather Service a decade ago, according to a study

published in the June issue of Weather and Forecasting, a journal of the American Meteorological Society.

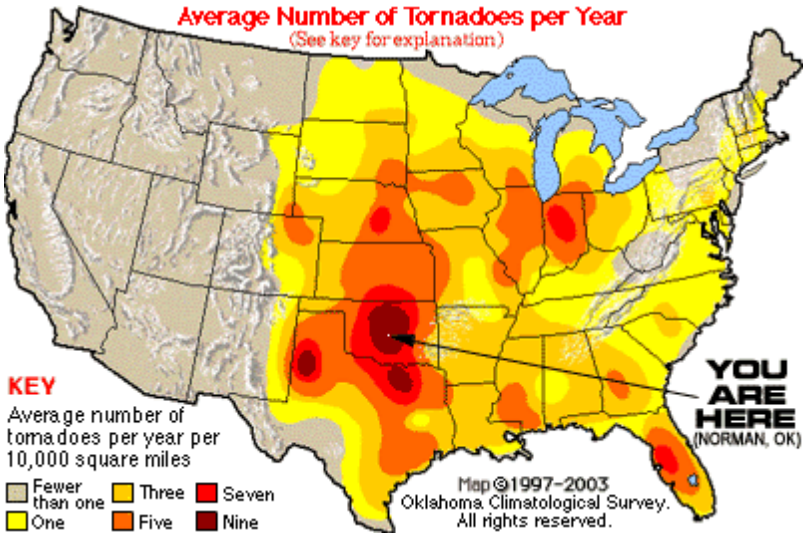

Figure 5. Average number of tornadoes per year

Researchers examined the impact of Weather Surveillance Radar-1988 Doppler (WSR-88D), also known as NEXRAD, which was installed in the 1990s during the National Weather Service's $4.5 billion modernization. They found the radars have significantly improved the quality of tornado warnings issued by NWS forecasters and lowered the number of tornado casualties nationwide. NEXRAD technology was developed at the NOAA National Severe Storms Laboratory.

The researchers, Kevin Simmons from the Department of Economics and Business at Austin College in Sherman, Texas, and Daniel Sutter from the Department of Economics and Cooperative Institute for Mesoscale Meteorological Studies at the University of Oklahoma in Norman, Okla., analyzed a dataset of tornadoes that occurred in the contiguous United States between 1986 and 1999. The date WSR-88D radars were installed at each National Weather Service Forecast Office was used to divide the sample for comparison.

The percentage of tornadoes warned for almost doubled - from 35 percent before WSR-88D installation to 60 percent after installation. In addition, the mean lead time of warnings increased more than four minutes, from 5.3 to 9.5 minutes (1986 to 1999).

The researchers also conducted a regression analysis of tornado casualties, which revealed expected fatalities and expected injuries were 45 percent and 40 percent lower for tornadoes occurring after WSR-88D radar was installed at NWS Weather Forecast Offices. Their analysis, which controlled for the characteristics of a tornado and its path, also found expected casualties were significantly lower for tornadoes occurring during the day or evening than late at night throughout the

sample. This provided indirect evidence of the life saving effects of tornado warnings.

"Anytime public money is used to invest in a technology like Doppler radar, it is important that we evaluate the results," Simmons said. "Our study provides strong evidence that this investment has had a significant effect on reducing injuries and fatalities from these storms."

Harold Brooks, Editor of Weather and Forecasting and research meteorologist at the NOAA National Severe Storms Laboratory in Norman, Okla., said, "This is the first effort to quantify the impacts of the radar on the core National Weather Service mission of protecting lives and property from severe weather."

Radars are a vital tool for the 122 National Weather Service forecast offices as they issue nearly 3,000 tornado warnings each year. The average warning lead time continues to increase and in 2004 was 15 minutes; part of this success is given by the improvement in tornado detection algorithms used by these WSR 88D.

With this information we might wonder if 15 minutes of lead warning time is enough, and how sometimes the NWS issues tornado warnings in some cases from one or two days before the occurrence or the Storm prediction center issues watches? The answer to that is not simple, according to john Edwards, from the Storm Prediction center: “When predicting severe weather (including tornadoes) a day or two in advance, we look for the development of temperature and wind flow patterns in the atmosphere which can cause enough *moisture, instability, lift, and wind shear* for tornadic thunderstorms. Those are the four needed ingredients. But it is not as easy as it sounds. How much is enough of those is not a hard fast number, but varies a lot from situation to situation -- and sometimes is unknown!”, he also implies that a large variety of weather patterns can lead to tornadoes; and often, similar patterns may produce no severe weather at all. To further complicate it, the various computer models they use days in advance can have major biases and flaws when the forecaster tries to interpret them on the scale of thunderstorms. Certainly 15 minutes is not much time to make major preparations therefore investigators are constantly working on increasing the lead time either with better understanding of weather phenomenon or with improvements over the field of tornado detection algorithms.

In this report we are going to address the current TDA (tornado detection algorithm) of the WSR 88D (hereafter NSSL TDA) and compare it to a new algorithm, NFTDA (neuro-fuzzy tornado detection algorithm). The result of this scoring is going to be provided quantitatively and qualitatively, and it should aid in the training process of the NFTDA. After this analysis we should be able to recognize the advantages and aspects that need to be reinforced in NFTDA in order to be a candidate to be the next operational TDA.

1. HISTORICAL BACKGROUND

We have already talked about the benefits of NEXRAD in the previous topic, now, we would like to give a historical background on the development of radars and its evolution.

Doppler radars have been used for nearly 50 years; in fact the first Doppler radar built for wind speed measurements was a continuous wave (CW) with a 3 cm wavelength (studies carried by Brantley and Barczys, 1957; Smith and Holmes, 1961). On June 10 1958, the Doppler velocity spectrum (weighted velocity distribution) from the radar indicated velocities up to 92 m/s in the developing funnel of a major tornado that struck El Dorado, Kansas, with a distance of 41 km relative to the position of the radar. One of the major improvements back at the time was the upgrading of the CW Doppler radar to Pulse Doppler radar (Lhermitte and Kessler, 1964). This technological change brought advantages such as range detection (although range detection in CW can be made by the use of chirping technique), measurement static objects (zero Doppler velocity), and overall, they can provide better resolution**,** but introduces a compromise between maximum detectable velocity and range, in other terms, velocity and range ambiguities, it is also more complex and therefore more expensive to build and maintain.

After more than 30 years of research on operational Doppler weather radar systems, the National Weather Service (NWS) began to deploy the **WSR-88D** in 1988. It replaced **WSR-74** and even **WSR-57** units from 1974 and 1957 respectively. The first installation was completed in the Fall of 1990 in Norman, Oklahoma, however, the first installation of a WSR-88D for use in everyday forecasts was in Sterling, Virginia on June 12, 1992. The last system was installed in North Webster, Indiana on August 30, 1997. The site locations were strategically chosen to provide the most overlapping coverage between radars in case one failed during a severe weather event. Where possible, they were co-located with NWS Weather Forecast Offices to permit quicker access to maintenance technicians.

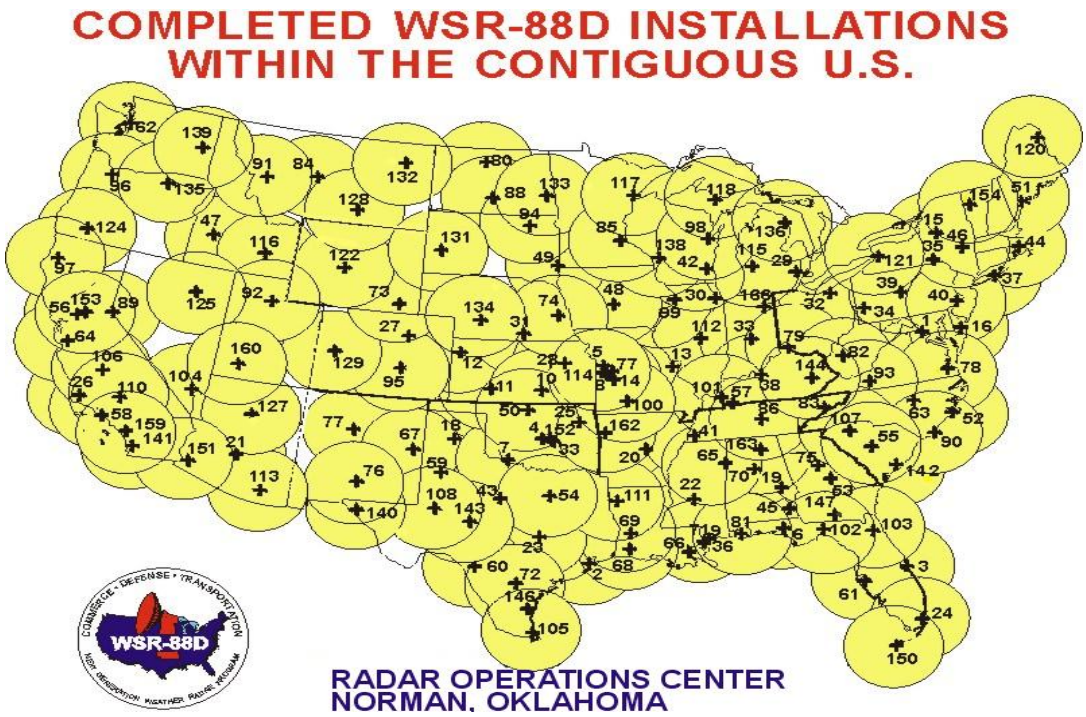

Figure 6. WSR 88D Coverage

This WSR-88D are used to warn the people of the United States about dangerous weather and its location. Meteorologists can now warn the public to take shelter with more notice than any previous radar. There are 158 operational NEXRAD radar systems deployed throughout the United States and at selected overseas locations as seen in figure 6. The maximum range of the NEXRAD radar is 250 nautical miles (463 Km). The NEXRAD network provides significant improvements in severe weather and flash flood warnings, air traffic safety, flow control for air traffic, resource protection at military bases, and management of water, agriculture, forest, and snow removal.

2. INTRODUCTION TO DOPPLER RADARS

Next we are going to discuss briefly how a radar works. Basically a radar consists of an antenna, a transmitter a receiver and a signal processing module. As seen on figure 7.

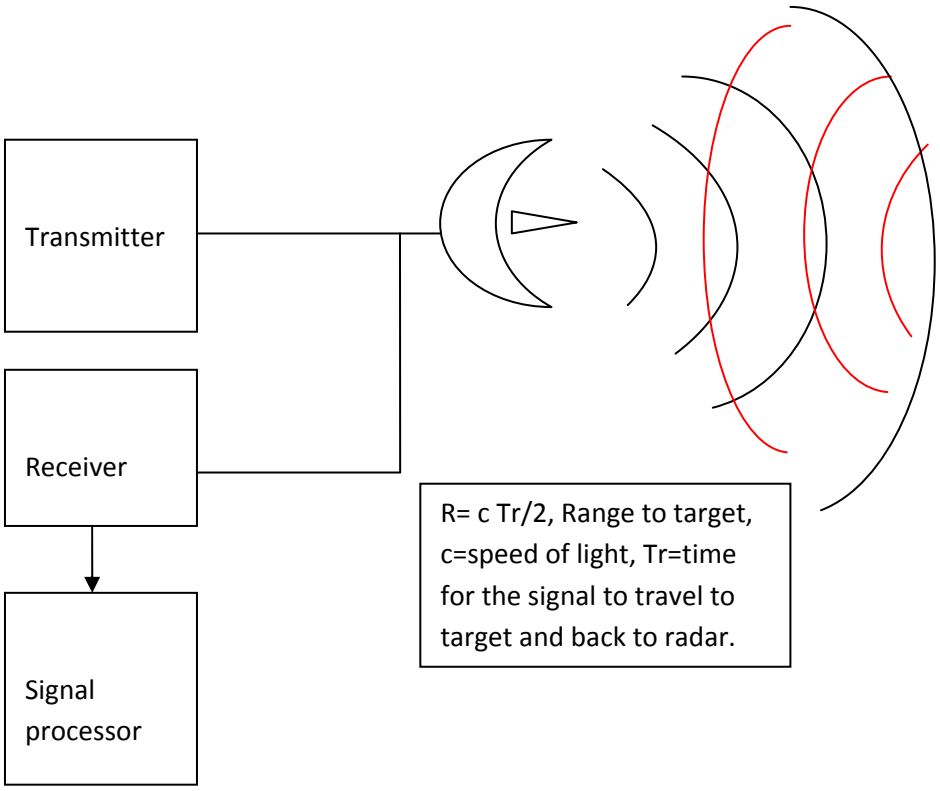

Figure 7. Basic radar block diagram

The transmitter produces an electromagnetic wave that propagates through the air, then it reflects on an object, and this object scatters back the energy (wave received) in many directions, part of this backscattered energy (wave) moves towards the antenna and the receiver identifies the signal and passes it to the signal processor, which will be in charge of obtaining information of a target according to the received signal. Of course, a radar would be much more complex and there are several constrains one must account for like propagations effects, scattering models, signal processing issues, clutter attenuation (suppression of unwanted returned signals), amongst others, none of them will be addressed since this is not under the scope of this report. From now on we will be discussing the most important characteristics of the WSR-88D, since these radars are the ones that provide the data we are going to use later in our report.

The WSR-88D radar is a coherent "chain-transmitter" design. Coherence, or phase information, in this type of design is maintained by very stable oscillators or signal sources that operate continuously. These sources are used as the reference in extracting the Doppler shift of the return signal, which is proportional to the radial motion of the target from which the transmitter signal is backscattered. A chain transmitter is one in which the transmitter signal is initially generated at a low power level, in this case a few hundred milliwatts, and increased to a high power, 750 kilowatts (kw), by an amplifier chain. Intermediate amplification is by solid-state devices and the final high-power amplifier is a klystron. The klystron is a vacuum tube device capable of high gain amplification (~60 dB) with negligible signal distortion or spurious emission. The antenna is a center-feed parabolic reflector having a diameter of approximately 28 ft (8.5 m). The antenna has a main lobe one-way 3 dB beam width of 0.93° at 2850 MHz (measured average), a first sidelobe level of 29 dB below the main lobe, a sidelobe taper greater than 1 dB per degree between 2° and 10° from the main lobe axis, and a far out sidelobe level more than 40 dB below the main lobe. The receiver uses two frequency mixers to down convert the received signal to zero frequency carrier (video signal). The first conversion generates an intermediate signal carrier at which most amplification, bandpass filtering, and automatic gain control (AGC) are done. The second frequency conversion is a synchronous detection (a detection that retains received signal amplitude and phase shift difference between received and transmitted signal phases but which removes the intermediate frequency carrier). At this point, the signal has an amplitude proportional to echo radar reflectivity and contains a frequency component equal to the Doppler shift. This is a "complex" signal; complex meaning that it contains both amplitude and phase information and, for convenience of handling and analysis, is decomposed into its vector components, i.e., two signals, inphase and quadrature, having a phase difference of 90° that, when added vectorally, form the complex signal.

The signal processors extract three meteorological quantities from the returned signal. These are: volume reflectivity, expressed in terms of equivalent radar reflectivity, Ze; the radial velocity, i.e., the component of motion of the reflecting particles toward or away from the radar; and spectrum width, which is a measure of dispersion of velocities within the radar sample volume. Reflectivity, Z, is calculated from the returned signal power and the known characteristics of the radar. Estimation is by a linear average of several return pulses, usually about 25, from each range cell. Velocity, v, is also estimated from several pulses (usually 40 to 50) pulses. The mathematical quantity computed is the return signal complex covariance argument using a technique called "pulse-pair processing" since the computation requires two pulses (two consecutive signal returns from the same target. Physically, the covariance argument provides a measurement of rotation rate of the complex vector representing the returned signal that is directly related to the Doppler frequency, Spectrum width, W, or velocity dispersion within the radar sample volume, is estimated indirectly. The computation performed is the returned signal autocorrelation which is related to the velocity spectrum standard deviation.

It uses the same pulses as radial velocit. These quantities are calculated by dedicated digital processors, i.e., processors designed and configured to perform a specific operation with only limited changes in parametric values.

The signal processor obtains first order products (RAW data) level 1 data, this then processed again and is stored on the NCDC Robotic Mass Storage System, commonly known as the Hierarchical Data Storage System (HDSS) at this point we get level 2 data (reflectivity, mean radial velocity, and spectrum width). Level 3 data consists of 41 products routinely available from NCDC. Most Level III products are available as digital images, color hard copy, gray scale hard copy or acetate overlay copies. Each copy will include state, county & city background maps. In order to obtain the needed data to feed the NFTDA and the NEXRAD TDA we must process it into a more familiar and easy to manage format. We chose the netcdf format since it can be read by matlab (with proper libraries installed). The process will be explained later in this report.

The most fundamental engineering characteristics of the WSR-88D are resumed in table 3 and 4

2.1 CHARACTERISTICS OF WSR 88D

2.1.1 Engineering characteristics, transceiver subsystem.

ANTENNA SUBSYSTEMS		
Radome	Rigid fiber glass	
Diameter	39 ft (12 meters)	
RF Loss – Two way	0.24dB at 2850 MHz	
Pedestal	Elevation over azimuth	
	Azimuth	Elevation
Steerability	360 °	+0.5 to +19.5
Rotational Rate- Maximum	30° / s	30° /s
Acceleration- Maximum	15 ° / s^2	15 ° / s^2
Mechanical Limits		-1° to 60°
Antenna	Paraboloid of revolution	
Polarization	Linear Horizontal	
Reflector Diameter	28 ft (8.5 meters)	
Gain (at 2800 MHz)	45 dB	
Beam Width	0.93° (at 2850 MHz, Measured Average)	
First sidelobe level	-29 dB	
TRANSMITTER AND RECEIVER SUBSYSTEM COHERENT – CHAIN DESIGN		

Transmitter	
Frequency Range	2700 MHz to 3000 MHz
Peak Power	750 Kw
Pulse Widths (nominal)	1.57 us and 4.5 us
RF duty Cycle	0.002 maximum
PRFs	Short Pulse : 318 Hz to 1304 Hz
	Long Pulse: 318 Hz to 452 Hz
Receiver	
Dynamic Range	93 dB
Noise Temperature	450°K
Intermediate Frequency	57.6 MHz
Band Width	0.63 MHz

Table 3. Engineering characteristics of WSR-88D, Antenna subsystems, transmitter and receiver subsystems.

2.1.2 Engineering characteristics, signal processor subsystem

SIGNAL PROCESSOR SUBSYSTEM	
Clutter	Infinite Impulse Response Design
Suppression	30 dB to 50 dB
Notch half widths	0 to 4 m/s
Intensity Bias	0 to 1dB
Minimum usable velocity	0 to 4 m/s
Range increment	0.25 KM (0.13 nm)
Azimuth Increment	1°
Velocity Calculation	Complex Covariance Argument
Algorithm	Pulse Pair processing
Estimate accuracy (nominal)	1m/s
Number of pulses averaged	40 to 280
Range increment	0.25 Km (0.13 nm)
Azimuth Increment	1°
Spectrum Width Calculation	Autocorrelation

Algorithm	Single lag correlation
Estimate accuracy (nominal)	1m/s
Number of pulses averaged	40 to 280
Range Increment	0.25 Km (0.13 nm)
Azimuth Increment	
Intensity Calculation	Return Power Average
Algorithm	Linear average
Estimate Acurracy (nominal)	1dB
Number of pulses averaged	6 to 64
Range Increment	1 Km (0.54 nm)
Azimuth Increment	1°

Table 4. Engineering characteristics of WSR-88D, Antenna subsystems, transmitter and receiver subsystems.

3. FUNDAMENTAL CONCEPTS OF A DOPPLER RADAR

A pulse Doppler radar, in its simplest form, is one providing a signal reference by which changes in the radio frequency (rf) phase of successively received pulses may be recognized. Such a radar is termed "coherent," i.e., it maintains rf waves with a continuous relationship among phases. The known phase of the transmitted signal enables measurement of the phase of the received signal. The Doppler shift associated with the echo from which the return originated is calculated from the time rate of change of phase.

The relationship between phase time rate of change and Doppler frequency can be visualized by considering the returned signal from a single target. The complex signal, i.e., inphase, I, and quadrature, Q, returned from a single target at a radial range, r, is of the form:

$$I = A\cos\left[\frac{4\pi r}{\lambda} - \Psi\right]$$

$$Q = A\sin\left[\frac{4\pi r}{\lambda} - \Psi\right]$$

Where:

A= signal amplitude (proportional to target cross-sectional area)

λ = radar wavelength

4πr / λ = phase due to range propagation of 2r (to the target and back)

Ψ =initial phase of the transmitter signal

If the range, r, changes with time (target moving relative to the radar), the argument, 4πr / λ−Ψ, becomes a function of time. Time rate of change of phase is the angular velocity, ω, expressed as:

$$\frac{d}{dt}\left[\frac{4\pi r(t)}{\lambda} - \Psi\right] = \frac{4\pi}{\lambda}\frac{d[r(t)]}{dt} = \frac{4\pi}{\lambda}v_r = \omega$$

Since time rate of change of range d[r(t)]/dt is radial velocity, vr, by definition. Since angular velocity, ω is related to frequency, f, by ω = 2πf:

$$2\pi\frac{2v_r}{\lambda} = 2\pi f_d$$

And the Doppler frequency fd is given by:

$$f_d = \frac{2v_r}{\lambda}$$

The angular rate of change is equal to 20 Hz per meter per second of radial velocity for a radar wavelength of 10 cm.

In summary, the fundamental transformations of meteorological characteristics to radar signal characteristics are: target cross-sectional area becomes proportional to signal power, target radial range becomes proportional to signal phase, and target radial velocity becomes proportional to time rate of phase change.

Thus, estimates of these electrical signal properties provide estimates of the corresponding meteorological properties.

Pulse radar is intrinsically a "sampled data system" since the measurement is time and space discrete. Time corresponds to the pulse repetition time (PRT) and space to the sample volume depth of the radar. The discrete time sampling results in a coupling between the maximum unambiguous range and the maximum unambiguous velocity associated with the radar and the discrete spatial sampling limits the scale that can be resolved by the radar.

3.1 MAXIMUM UNAMBIGUOUS RANGE

The maximum unambiguous range, ra, i.e., the maximum range to which a transmitted pulse wave can travel and return to the radar before the next pulse is transmitted, is simply:

$$r_a = \left[\frac{c\ PRT}{2}\right]$$

Where c is the wave propagation constant (speed of light).

3.2 MAXIMUM UNAMBIGUOUS VELOCITY

Discrete time sampling, i.e., sampling at the radar PRT interval, also limits the maximum frequency that can be resolved. This is given by the Nyquist Sampling Theorem and is somewhat involved, but the mechanisms and implications can be understood by the following considerations.

The Nyquist frequency, fn, is the highest frequency that can be resolved by Δt spaced samples. It is given by fn = $1/(2\Delta t)$ and corresponds to two samples per cycle on a sinusoid of fn.

Sampling of frequencies higher than fn results in an "aliasing" by which frequencies higher than fn appear in the range from zero to fn. Sampling of frequencies less than and greater than fn is illustrated in figure 8.

3.3 DOPPLER DILEMA

Consider the case shown in figure 8.a where a frequency of 166 2/3 Hz is sampled every one thousandth of a second (a 1000 Hz rate) and the extrapolated output is a frequency of 166 2/3 Hz, i.e., same frequency as the input. Consider now the case shown in Figure 8b where a frequency of 833 1/3 Hz (above the Nyquist frequency) is sampled at a 1000 Hz rate. The extrapolated output frequency is equal to the sampling frequency, 1000 Hz, minus the input frequency of 833 1/3 Hz, which yields a frequency of 166 2/3 Hz.

The limitations on maximum unambiguous frequency, fn, imposed by the sampling rate fs = 1/PRT results in "coupling" between unambiguous frequency (velocity) and unambiguous range since both are functions of radar PRT. Since:

$$\frac{2v_a}{\lambda} = f_n = \frac{1}{2}\frac{1}{PRT} \quad and \quad r_a = \frac{c\,PRT}{2}$$

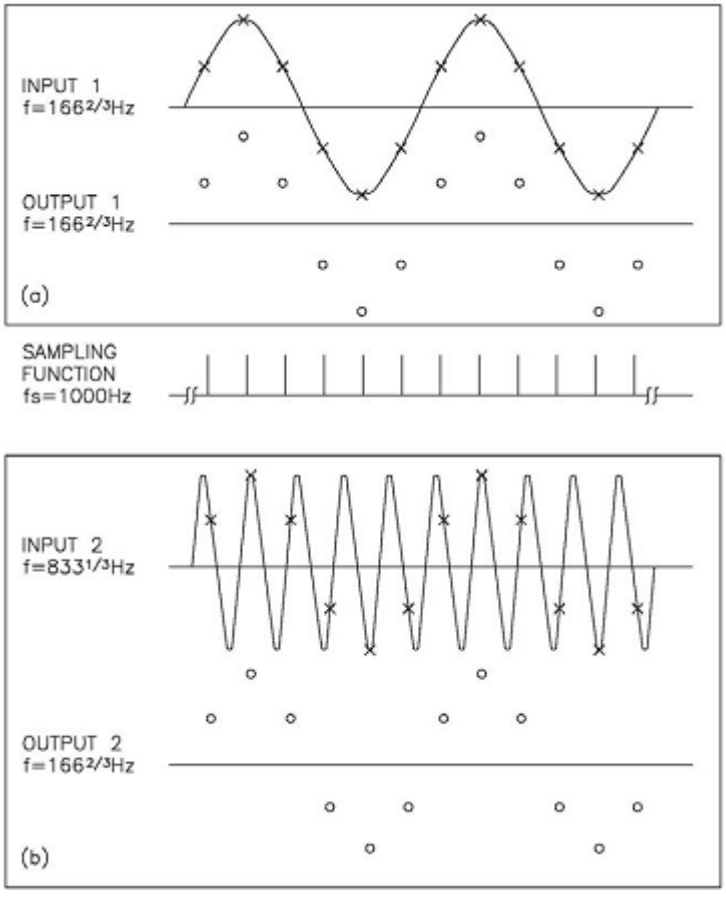

Figure 8. Example of sampling of a signal.

Thus,

$$r_a v_a = \frac{c\lambda}{8}$$

Where:
va= unambiguous velocity
ra= unambiguous range

Thus, the product of unambiguous range and unambiguous velocity is a constant determined by the wavelength of the radar (refer to figure 9).

In figure 9, dashed lines are for unambiguous velocities of 30, 25, and 20 ms-1 with associated unambiguous ranges of 134, 160, and 200 km.

The range-velocity coupling is probably the most important operational constraint of the WSR-88D since it results in the operational problems of range folding and velocity aliasing.

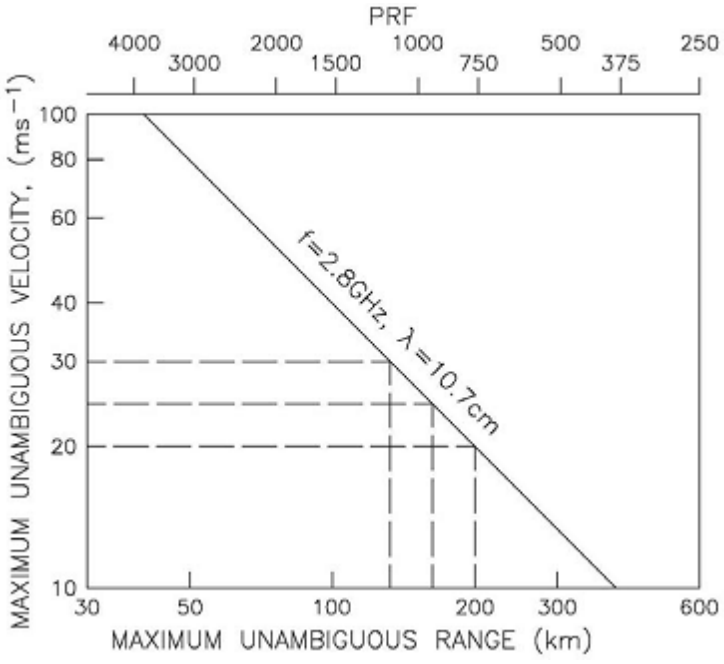

Figure 9. Unambigous Range-Velocity relationship for the WSR 88D.

3.4 ESTIMATE VELOCITY ON DOPPLER RADARS

The velocity measurement technique used in the WSR-88D is essentially a method of Doppler angular frequency measurement, i.e., measurement of ω = 2πf in a time-varying function of the form y = cos ωt. This is equivalent to a measure of velocity since frequency is linearly related to velocity by the Doppler equation.

The actual computation is a minimum-variance, unbiased estimation of the complex covariance of the Doppler signal represented by the inphase, I, and quadrature, Q, video signals (a complex signal is needed to measure the sign of the Doppler frequency, i.e., whether the frequency shift is above or below the transmitted signal corresponding to velocities toward or away from the radar).

The estimate of velocity (v) is:

$$v = k\,Arg\sum_{n=1}^{N-1}[Z_{n+1}Z^*_n]$$

Where
K= a constant specified by X and PRT
Arg[]= the argument or angle of the quantity
Z=a complex singal of the form Z=I+jQ
Z*= complex conjugate of Z
n=sample sequence index
N= total number of samples

Due to the discrete nature of the sampling, the angular velocity of the vector represented by Z is measured as a differential. For example, given the vector Zn = 3 + j3 in the first quadrant as shown in figure 10a, assume that, by one PRT later, the next sample, Zn+1 = -4 + j2, appears in the second quadrant corresponding to a displacement between samples of 108 degrees. The complex multiplication of the second sample, Zn+1, and the conjugate of the first Z*n produces a vector (Zn+l Z*n) magnitude equal to the product of magnitudes of Zn and Zn+l with an angle equal to the difference in angles of Zn and Zn+1 or the displacement of the vector over the radar PRT as shown in figure10b. Angular velocity is thus ω = (θn-1 - θn)/PRT.

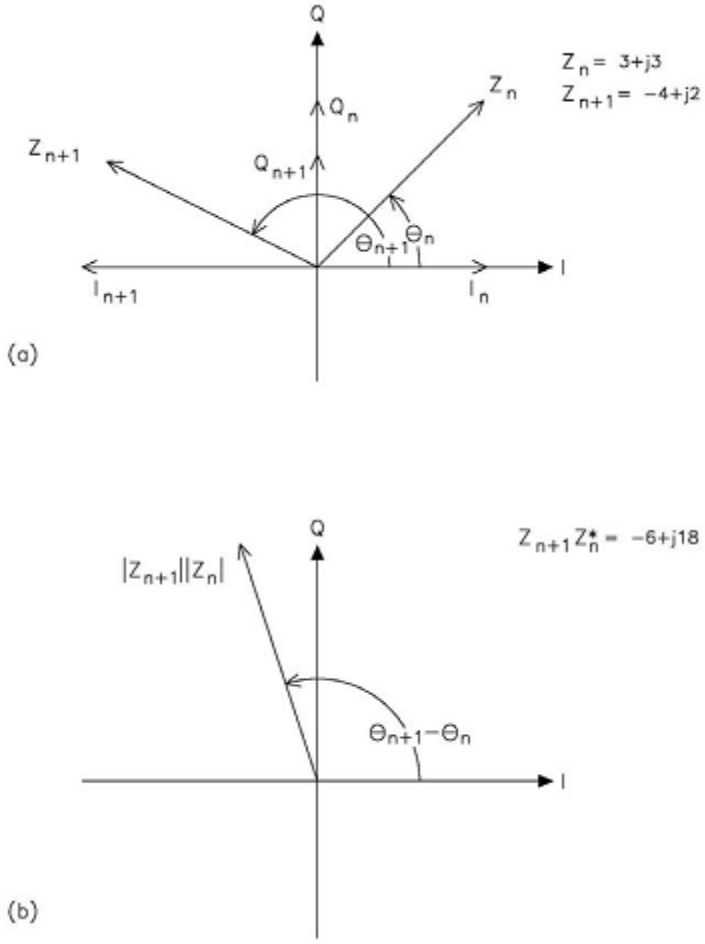

Figure 10. Velocity sampling. a. vector representation of two consecutive complex video samples (I,Q). b. result of the complex multiplication Zn+l Z*n.

The summation, as shown in figure11c, produces a mean displacement in which the individual displacements are weighted by the product of the two vector lengths (power of the signal) and the mean velocity is estimated from the power-weighted, average vector displacement.

Using the linear relationship between phase displacement and velocity, figure 11d illustrates what occurs when the input velocity vT, corresponding to θT, exceeds the unambiguous velocity, ±va, corresponding to + π. When the true displacement is greater than + π, but less than + 2π principal angle detection, θm corresponds to a measured velocity, vm, having a magnitude |vm| = 2va - |vT| and with a sign opposite that of vT.

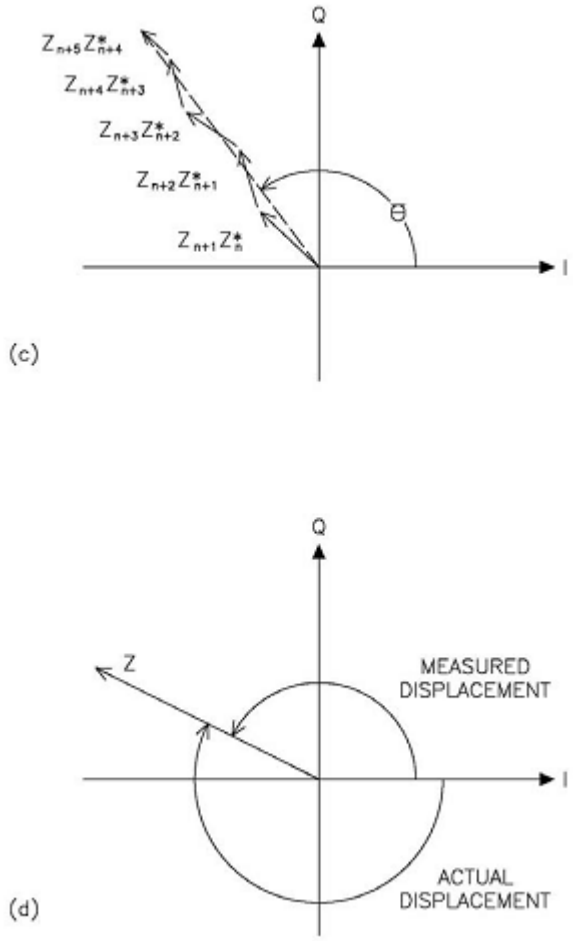

Figure 11. Velocity sampling. c. Schematic of vector summation. d. frequency aliasing in the complex plane.

The uncertainty of the velocity estimate, i.e., how well the estimate represents the true mean velocity values, is dependent on input spectrum width--the larger the width the larger the uncertainty. Estimate accuracy can be improved or uncertainty reduced by increasing the number of samples in the estimate. Figure 12 gives the estimate accuracy or standard deviation, SD[v], (the measured velocity will be within + one standard deviation of the true velocity 63% of the time) as a function of spectrum width with signal-to-noise ratio as the parameter of variation for unambiguous velocities representative of the WSR-88D.

It is seen from figure 12 that the estimate of the standard deviation is dependent on unambiguous velocity, va, input spectrum width, W, signal-to-noise ratio (SNR), and the square root of the number of samples in the estimate (NI/2).

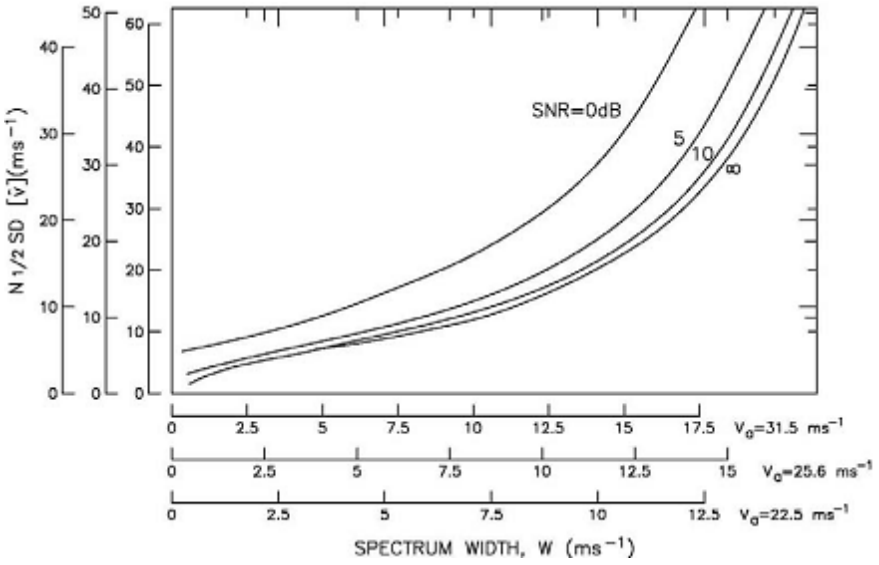

Figure 12. Standard deviation of the mean velocity estimate.

This figure depicts the normalized standard deviation of the mean velocity estimate as a function of spectrum width for three unambiguous velocities and four levels of signal-to- noise ratio (SNR). Note the ordinate value must be divided by N1/2, the square root of the number of samples in the estimate.

For example, the WSR-88D with wavelength of 10 cm and a pulse repetition frequency (PRF) of 1 kHz [va = 25 m/s], operating at an antenna speed of 3 rpm, delivering estimates on a l° polar grid (55 samples per estimate), and viewing a meteorological target having spectrum width of 5 m/s at a signal-to-noise ratio of 10 dB delivers a standard error of mean Doppler velocity estimate of 1 m/s.

In summary, the mean Doppler velocity estimation technique used on the WSR-88D is a vector calculation of the time rate of change of signal phase that is converted to velocity through radar system constants (λ, PRT). The calculation operates in the continuum of vector space from 0 to ± π that provides a smooth transition through the Nyquist frequency or maximum unambiguous velocity. Measured velocities, vm that are aliased, appear as the difference between, +2va, and the true velocity, vT, i.e. vm = 2va - vT. Examination of the figure 12 reveals that meteorological parameters influencing estimate standard deviation for a given radar setup are spectrum width and SNR. For a given signal-to-noise ratio, the standard deviation of the velocity estimate increases as the square root of input spectrum width up to widths of about 0.4va. At larger spectrum widths, the standard deviation of estimate increases very rapidly (loss of signal coherency) and becomes unacceptable for widths greater than about 0.5va. Noise influence on estimate accuracy is negligible for SNR>10 dB. However, the increase in

standard deviation increases very rapidly for SNR<10 dB and becomes unacceptable in most cases for SNR<0 dB.

4. TORNADO DETECTION ALGORITHMS EVOLUTION

It is important to emphasize that Doppler radars have a limited range of radial velocities that they can observe. Velocities beyond that range will be "folded" back into that range such that a strong outbound velocity, just beyond the observable range, will be interpreted as a strong inbound velocity within the observable range.

A high pulse repetition frequency (PRF) pulse Doppler radar is optimal for tornado studies, since it would increase the sampling rate (as given by the Nyquist Sampling theorem) and avoid velocity aliasing, but it would have lower maximum range detection as we saw before.

Next we are going to overview how Tornados are seen from a radar point of view.

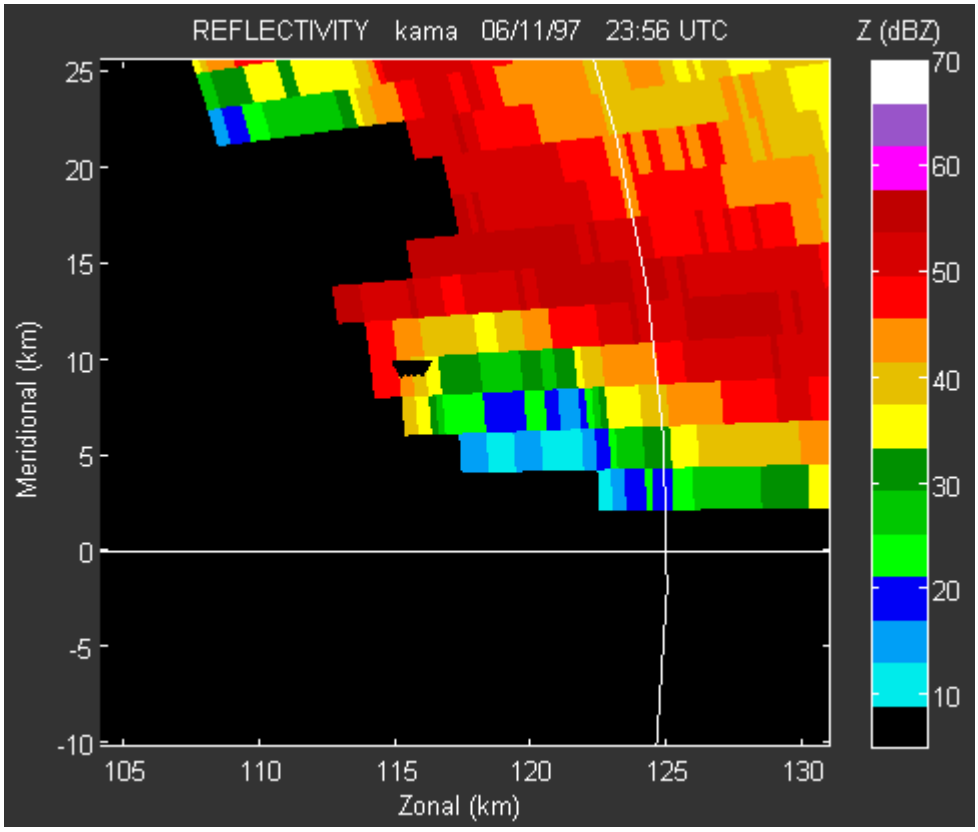

Figure 13. Reflectivity ppi (plan position indicator) plot, graphs provided by software developed by the author.

The hook echo is seen for this case by kama radar Amarillo,Texas on june 11 1997. (Elevation: 0.5 deg).

On figure 13 we have the PPI plot of the Reflectivity (backscattered proportional energy received at the antenna) for the case of a tornado on Grey County from Amarillo texas “kama” radar, june 11 1997. We notice how the hooked shape figure forms on the plot (red curve that involves the yellow green and blue shades), this characteristic is found on several tornadic cases, but is not necessary in all, and thus not completely reliable. Forbes et al. 1981 gathered a data base consisting of several cases that occurred during 3rd april 1974, his conclusions where that some of the tornadoes did not exhibited the hook echo or another distinctive reflectivity echoes. He also concluded that even though the hook echo can sometimes correlate to the tornadic event, it does not provide sufficient lead time for tornado warnings and high false alarm rate can occur.

On the Oklahoma City tornadic storm of May 24 1973 (brown 1976) detailed scrutiny of Doppler velocity spectra by burgess et al 1975 b, discovered a unique mean of Doppler velocity signature, the Tornado vortex signature (TVS). This signature has been seen in several storms and is the starting point for current tornado detection algorithms. As an example, on figure 14 we can observe the velocity field plot of the Gray case on june 11 1997. We notice the high inbound velocities with respect to radar colored in red, and the high outbound velocities with respect to radar colored in green, this is evidence of rotation.

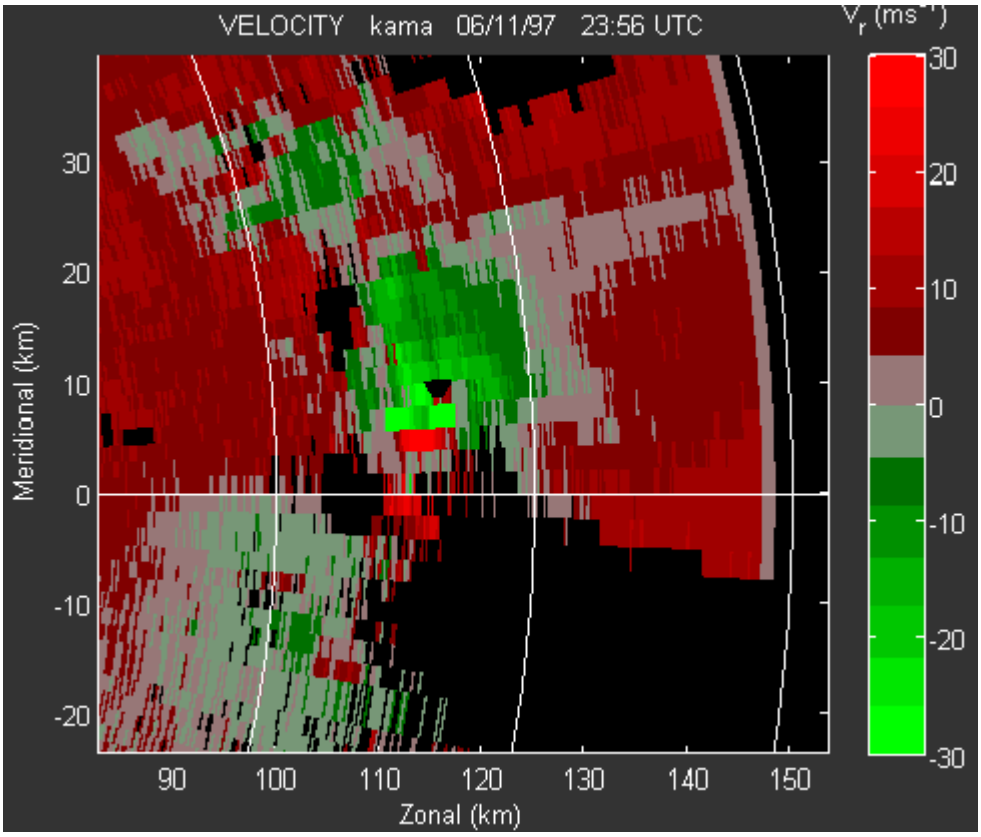

Figure 14. TVS observed by kama radar Amarillo,Texas on june 11 1997. Velocity PLOT (elevation: 0.5 deg), graphs provided by software developed by the author.

This TVS provided a framework for the design of the 88D TVS algorithm (Crum and Alberty 1993) but had a low POD (probability of detection) compensated with a low FAR (false alarm rate), (Mitchell et al. 1997), the NSSL (national severe storms laboratory) in conjunction with the FAA and the NWS operational support facility (OSF) developed an enhanced algorithm to address the low POD of the 88D TVS without an extremely FAR, the result is the current tornado detection algorithm which is operational throughout the NEXRAD (WSR-88D's) hereafter: NSSL TDA.

5. CONSIDERATIONS ON DOPPLER RADARS

Until now we have discussed how the WSR-88 are composed, how the different measurements are obtained from the receiving signal and how tornadoes are seen on radars on an ideal sampling situation. In practice, ”ideally” does not exist, thus, we will make a brief recap on some of the issues that might compromise the detection of a tornado by the WSR-88D (and most Doppler radars).

The following definitions apply (brown et al. 1997):

5.1 DEFINITIONS

1) Tornado signature—a rare vortex signature of extreme Doppler velocity values (of opposite sign) separated by at least several beamwidths in the azimuthal direction, which arises when the tornado is within a few kilometers of the radar and the tornado is larger than the radar beam;
2) tornadic vortex signature (TVS)—a vortex signature of degraded Doppler velocity extremes (of opposite sign) separated by about one beamwidth in the azimuthal direction, which arises when the radar beam is wider than the tornado; characteristics of the tornado are degraded to such an extent that neither the size nor strength of the tornado is recoverable (Brown et al. 1978);
3) mesocyclone signature—a vortex signature of extreme Doppler velocity values (of opposite sign) separated by approximately 3–10 km in the azimuthal direction, that arises when the mesocyclone is larger than the radar beam;
4) mesocyclonic vortex signature—analogous to the TVS, a vortex signature of degraded Doppler velocity extremes (of opposite sign) separated by about one beamwidth in the azimuthal direction, which arises at far ranges when the radar beam is wider than the mesocyclone’s core diameter; characteristics of the mesocyclone are degraded to such an extent that neither the size nor strength of the mesocyclone is recoverable.

A thorough understanding of WSR-88D Doppler radar sampling issues is crucial for proper identification and assessment of severe thunderstorm signatures. Sampling issues include radar horizon, scan strategy, beam width versus range, aspect ratio, and range folding. While the WSR-88D is a very powerful and sensitive radar, changes in storm appearance can still occur as storms approach or move away from the radar due to these problems. Thus, unless radar sampling issues are understood, improper signature interpretation could occur. However, once understood and accounted for in displayed radar data, proper analysis is likely.

5.2 RADAR HORIZON

The radar horizon presents a problem for viewing storms as they increase in range from the radar data acquisition (RDA; i.e., antenna). The radar beam increases in height with range due to the earth's curvature. Thus, for finite depth phenomena, such as mesocyclones, the chances of the radar beam overshooting the phenomena increase with increasing range (Figure 15). Also, the same storm viewed by several radars will produce different storm appearances, especially if the same elevation angles from each radar are used. Figure 16 shows a plot of height versus horizon distance, taking into account each elevation angle of a radar scan.

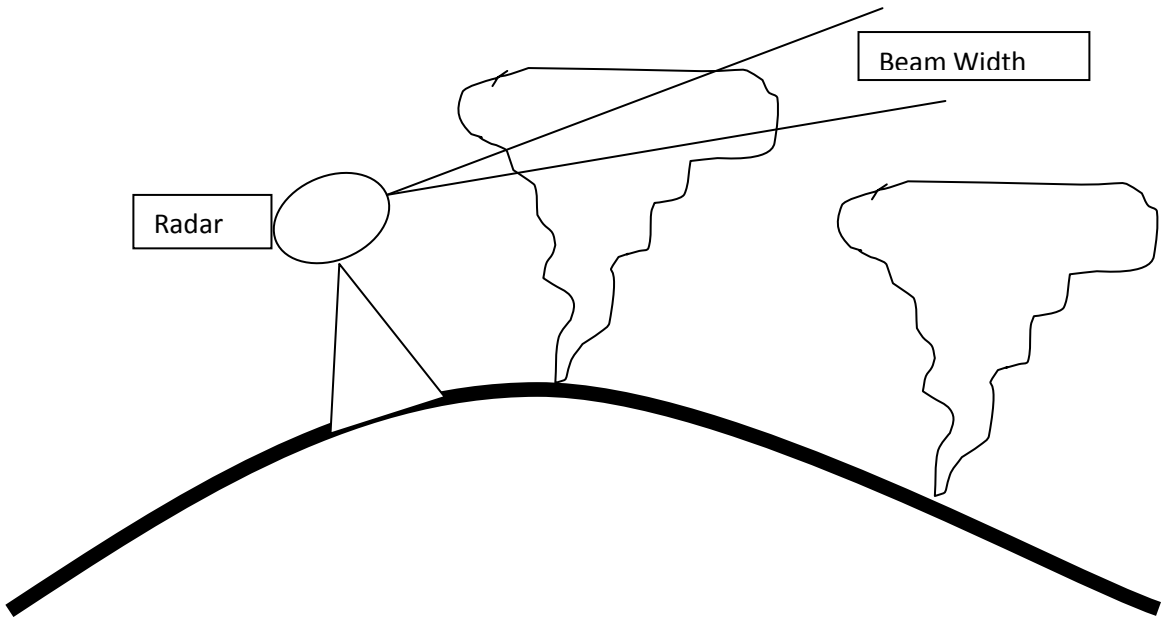

Figure 15. Idealized example of the radar horizon problem.

The bold line is the exaggerated curvature of the earth. The curly outline represents a thunderstorm.

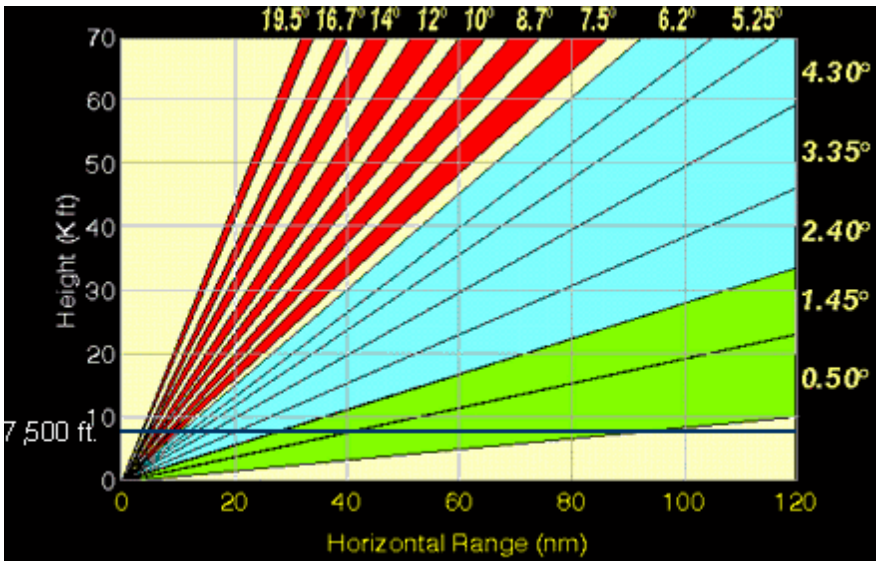

Figure 16. Different scan angles of WSR-88D and its respective height and range

A 7500 ft circulation can be easily resolved by the radar at 20 nm, but at 100 nm it would be very hard. Graph provided by the Oklahoma Climatological survey 2000.

5.3 SCAN SRATEGY

Scan strategy affects sampling of thunderstorms. Volume Coverage Pattern (VCP) 11 (14 elevation angles scanned in 5 minutes) contains higher slices than VCP 21 (9 angles in 6 minutes), which allows better assessment of the middle and upper levels of convection close to the radar. The lowest several slices of VCP 11 and 21 are identical. However, VCP 21 usually is a little more accurate at velocity data retrieval than VCP 11 given its slower antenna rotation. With either VCP, the radar operator must view the "correct" elevation angles to detect key features within a storm. Four-panel displays are useful for this purpose.

For storms close to the radar, it is probably best to use VCP 11, which will allow evaluation of features higher in the storm and allow better volume products such as VIL, mesocyclone, echo tops, and vertical cross-sections. VCP 11 also allows slightly faster data availability than VCP 21, which is important for rapidly moving or changing storms. For distant storms, VCP 21 may be better since the lowest several elevation slices likely will allow evaluation of the entire storm depth, while

permitting the best possible velocity data retrieval. No matter what VCP is used, it is crucial that the low- and middle-levels of a storm be sampled, since features at these altitudes are closely related to severe weather at the surface. Storm-top divergence also may be important. Again, use neighboring radars for distant storms to view the lower levels.

5.4 BEAM WIDTH VS RANGE

A fundamental concept of radar is that the radar beam becomes wider with range (figure 17). The beam width for the WSR-88D is 0.96 resulting in a beam diameter of about 2 nmi at 124 nmi from the radar (not that much). The definition of the edge of a radar beam is where the power lowers to one-half (the "half-power point") that of the beam centerline . Some information, especially for velocity estimates, may be returned from side lobes outside the defined radar beam. Since the beam increases in width with increasing distance, velocity estimates likely will experience more averaging with range, since varying wind speeds within a sample volume (radar beam) are being used to calculate the radar displayed pixel value. In addition, reflectivity data will appear squarer shaped due to a wider beam, thereby decreasing the retrieved resolution of important reflectivity signatures at far out ranges. In addition, dBZ values may be averaged to slightly less than reality.

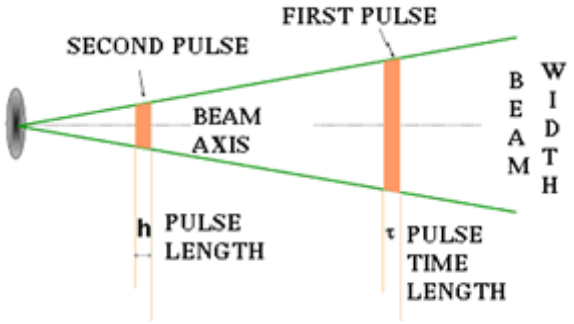

Figure 17. Beam width vs range expantion on increasing range

5.5 ASPECT RATIO

Aspect ratio deals with the beam width versus range problem. Aspect ratio is the ratio of the actual physical size of a particular precipitation or flow field entity (tornado, mesocyclone, hook echo, etc.) to the size of the radar beam. If the phenomena is very small compared to the sample volume, then the phenomena could essentially be invisible to or more likely not well sampled by the radar. Conversely, a large feature compared to a smaller beam (closer to the radar) would result in a more accurate presentation of the feature.

On figure 18, we can see a sample circulation sample on different range locations, the first circulation can be resolve, the second are averaged to read a velocity of zero and in the third the velocities are degraded since it is contained on a resolution bin and no circulation is apparent.

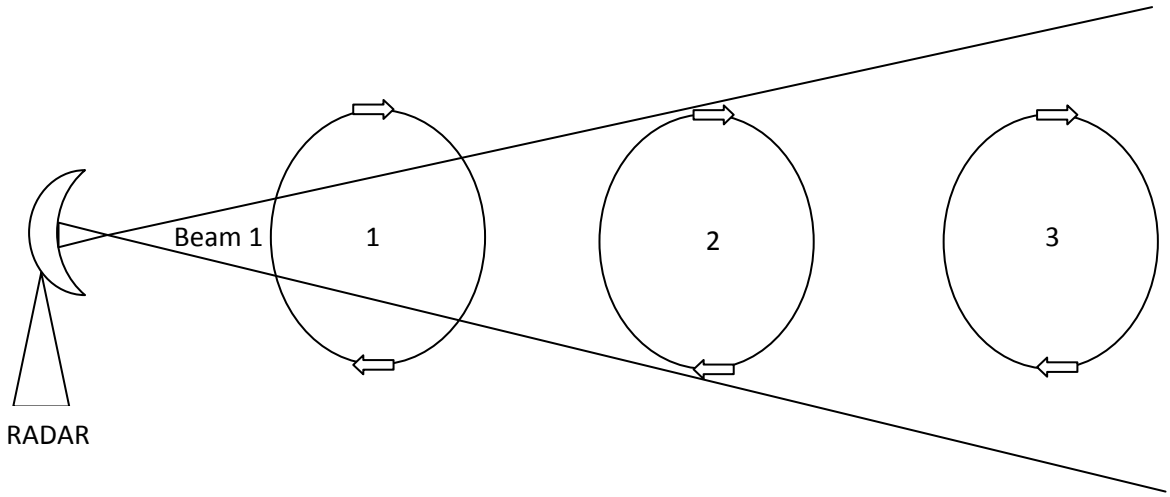

Figure 18. Sampling for a circulation of sample characteristics, but different range locations.

Exhibit 13 shows the circulations centered on the broad side of antenna, but the situation gets worse when the circulation is detected in different resolution bins. Ideally the circulation should be centered as exhibit 14 shows, in that way velocities are slightly degraded and a very good velocity estimate can be found. Exhibit 14 shows the scheme and the resulting WSR-88D display (bottom figure at right) would show symmetric "gate-to-gate" shear in two adjacent pixels (radar beams), one with inbound (minus sign) and one with outbound (plus sign) velocities. Due to a wider beam width at long distances from the radar, displayed radar velocities would be averaged a little lower than actual mesocyclone velocities.

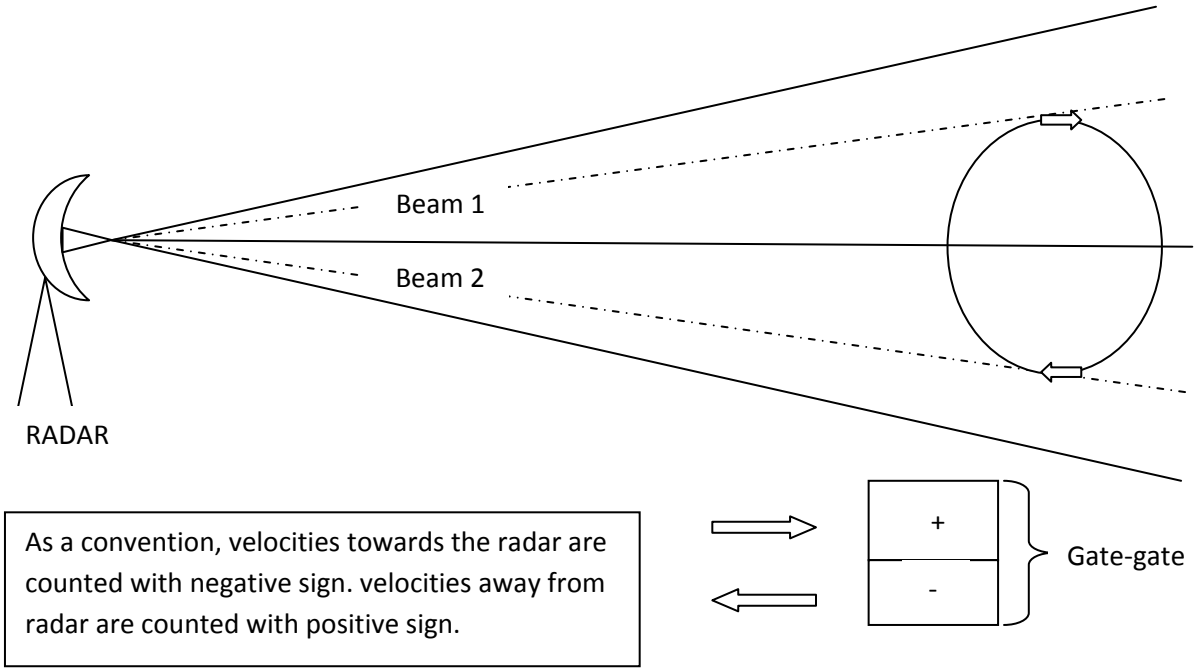

Figure 19. Idealized example of two adjacent radar beams from the RDA (radar site) sampling a mesocyclone (bold circle; top figure).

Here, the beam center line (dashed line; maximum beam power axis) intersects the edges of the solid body rotation core where maximum inbound and outbound velocities are found.

As see from figure 19, the positioning of the event according the radar "sampling bins", is crucial on obtaining accurate velocity measurements.

Brown et al. 1997 described this effect with axisymmetric Rankine combined vortex (e.g.,Brown and Wood 1991), which shows the same results we talked about previously.

5.6 RANGE FOLDING

This is a problem than could adversely affect interpretation of features in velocity and spectrum width data. Areas of range folded data (purple haze) can occur in any location where reflectivity is being returned from a variety of ranges along the same radial. This is of particular concern beyond the maximum unambiguous range (Rmax) for the given pulse repetition frequency (PRF). However, strong storms should still return enough power to generate useful data within the range folded area. By changing the PRF, the Rmax also will change, allowing possible visualization of an important feature. Decreasing the PRF will increase Rmax. Look

at other elevation angles using the primary radar and dial into other radars if possible to alleviate any range folded problem.

6. NSSL TDA AND DOWNSIDES

We have previously introduced the NSSL TDA when we talked about tornado detection algorithms evolution. Now we would like to expand this topic further to address the comparison of NSSL TDA and NFTDA with a better perspective.

The NSSL TDA algorithm is summarized in figure 20.

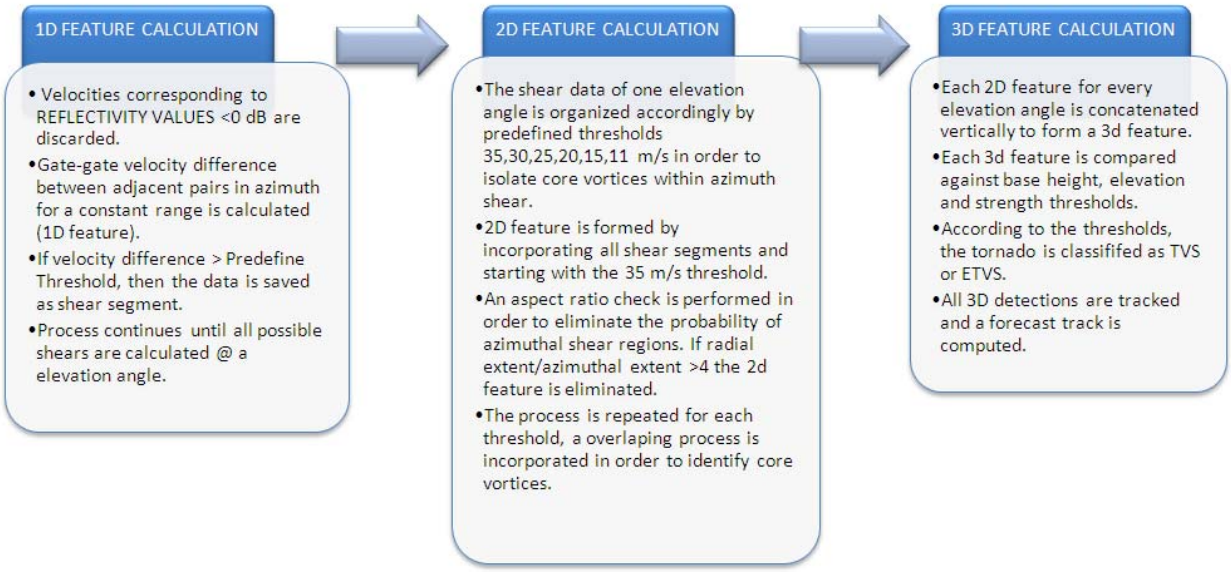

Figure 20. Summarized NSSL TDA

The NSSL TDA relies on the tvs, in the sense that it predicts the formation of a tornado based on the adjacent gate-to-gate velocity differences called shear (azimuthal shear), thus as we saw earlier, it becomes difficult to identify a tornado if it is far away or if its weak.

There are several solution that can tackle this problem

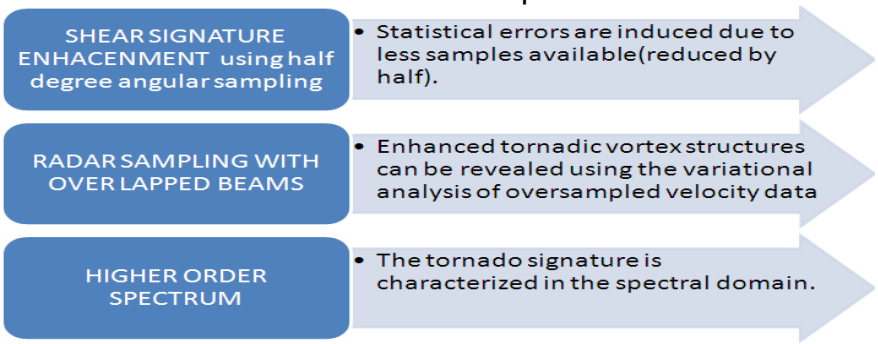

Figure 21. Posible solutions for NSSL TDA downsides.

7. NFTDA AND ITS STRENGTHS:

The primary concern that one should have regarding the NSSL TDA is it's dependence on individual thresholds on reflectivity and shear (gate-gate velocity difference). Wang et al. has shown that this parameters are overlapped on over another and should be treated ideally as fuzzy variables as depicted on figure 22.

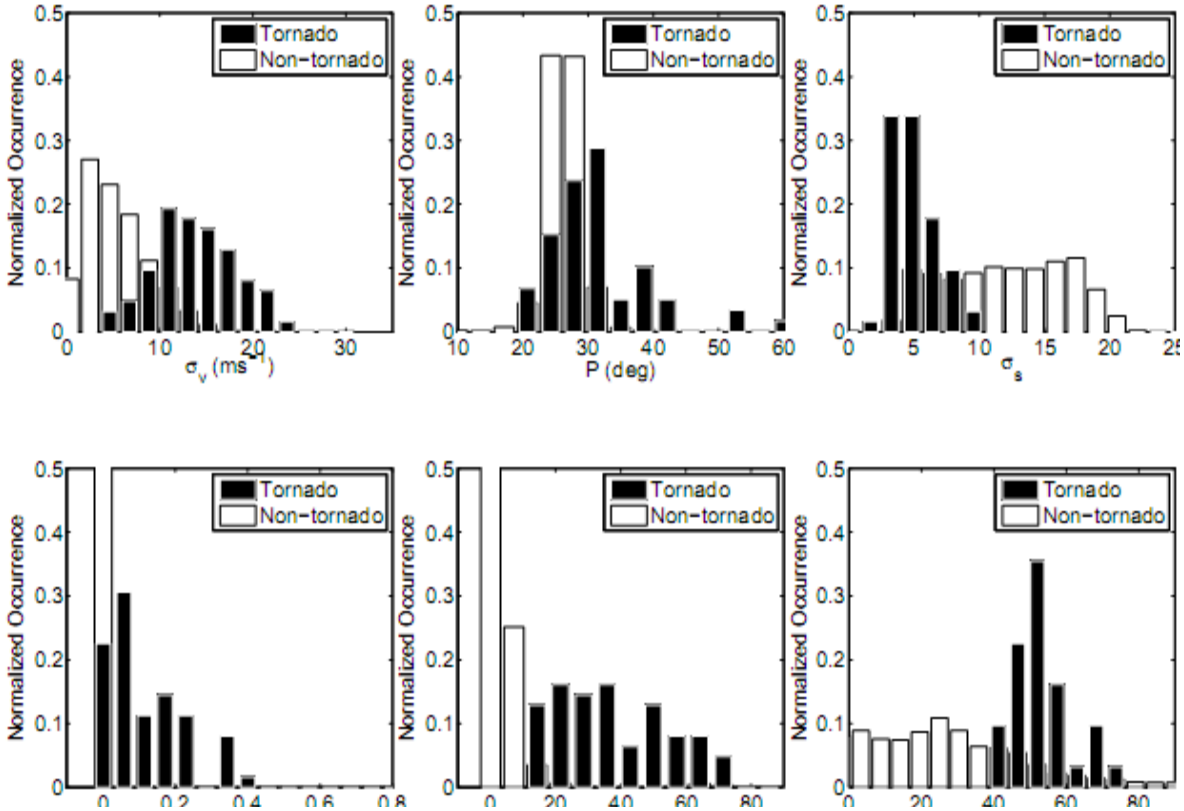

Figure 22. Normalized histogram of spectrum width (upper left), P value (upper middle), spectrum variance (upper right), eigen-ratio (lower right), velocity difference (lower middle), signal to noise ratio (lower right) for tornado and non-tornado regions.

NFTDA relies on 5 input parameters as we can see in figure 22 and 23, Spectrum width, spectrum variance, eigen-ratio, velocity difference, phase of the radially integrated bispectrum (PRIB), as described by Yu Et al. 2007.
It is shown that tornadoes are characterized by strong shear, large spectrum width, significant Eigen ratio, high PRIB and low value of spectral flatness, as described by Wang et al. As shown in figure 22, these parameters are also overlapped and must be addressed with a certain degree of fuzziness.

Figure 23 shows the NFTDA flowchart. Let us note that for this report we will be using the velocity difference, reflectivity and Spectrum width input parameters.

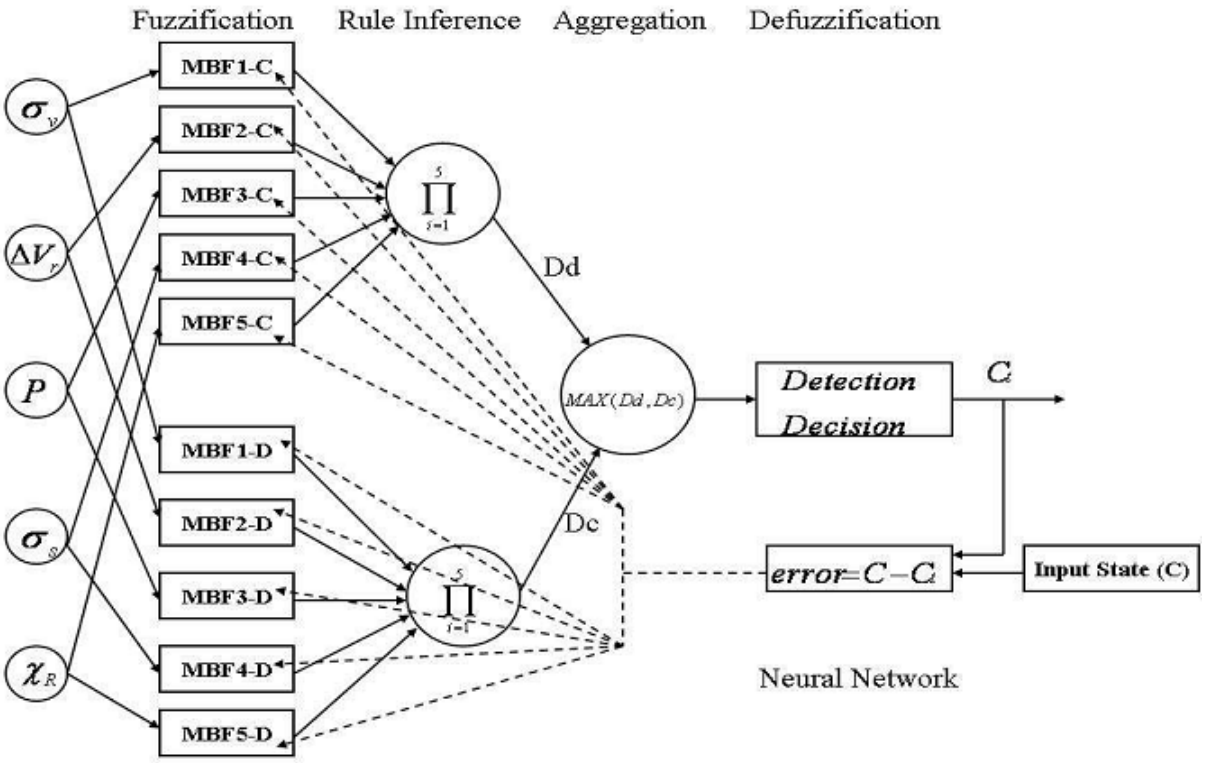

Figure 23. NFTDA Flow chart

The input parameters are turned evaluated in membership functions, then comes the rule inference which is a simple product of values from the different fuzzification procedure, after this we obtain a binary result after evaluating which case is higher as seen on figure 23. Dd and Dc are values for “detection” or “no detection”. A neural network is used to train the membership functions in order to obtain optimal thresholds.

8. DATA SET

The data used for this report was obtained from ground truth files which were used for the development of the WDTB Tornado Warning Guidance statistics.

The WDTB team took the tornado reports from *Storm Data* and "adjusted" them to better fit the locations of the attendant radar signatures.

The storm reports are somehow inaccurate due to many errors in position and time of the event. As a rule we took the reports that occurred over high population areas and the ones that corresponded better in range with the respective tornado detections by both algorithms.

The initial database consisted on 1500 tornadoes from different sites around the United States; these cases were carefully studied more than once in order to provide a better suited ground truth database for algorithm comparison purposes.

The dataset is in text form, and it had to be converter in to a digital form so that it could be ingested properly into the comparison algorithm. As a result we had the comparison algorithm managing all the complete scoring process.

9. SCORING METHODOLOGY

This was accomplished by associating multiple algorithm predictions (over a specific period of time or number of volume scans) with a single severe report. We defined:

$$POD = \frac{a}{a + c}$$

$$FAR = \frac{b}{a + b}$$

$$CSI = \frac{a}{a + b + c}$$

Where a, b, c are HITS, FALSE ALARMS, and MISES respectively and POD represents the probability of detection, FAR represents the false alarm rate and CSI represents the Critical success index.
HIT: correct detection per scan during time window.
MISS: no detection per scan during time window.
FALSE ALARM: detection per volume scan not associated with a tornadic event.

9.1 SPATIAL CONSIDERATION

We created a 15 km buffer around the ground truth data so that any detection outside this range will not be counted; this applies for HITS, MISSES and FALSE ALARMS. Another consideration arouse when for a given volume scan more than one algorithm prediction is generated for a small area (eg. For the same storm or county or even contiguous in range or azimuth and with the same time stamp), we took the closest detection with respect to the ground truth and discarded the other predictions. Also if a studied detection is closer to another tornado different than the studied, it will count only for the closer in range tornadic event. This will be seen more clearly in the next examples.

9.2 TIME CONSIDERATION

We created a time window form -15 minutes to +5minutes the occurrence of the event. As seen on figure 24.

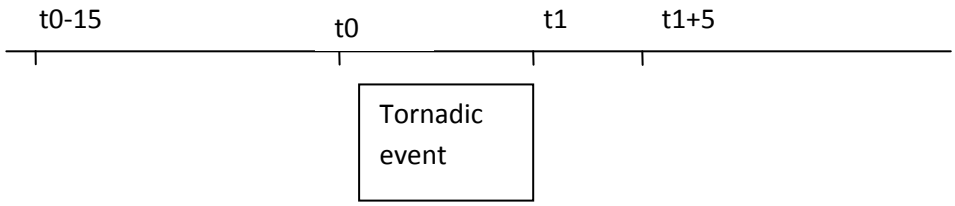

Figure 24. Time window scoring used, 15 minutes before and 5 minutes after event, all of this is within a 15 km buffer in all directions with respect to ground truth.

We also selected the NSSL TDA algorithm to provide a categorical “yes” for probabilities greater or
equal than 50% and a c

ategorical ‘’no” from 0 to 49%.
In situations where severe reports do occur at relatively high frequency or density, time windows from separate reports will occasionally overlap with the same algorithm prediction, leading to duplicate hits and misses, this duplicates where discarded so as to avoid producing artificial biases in the performance statistics.

Even though this scoring methodology is not the optimal, since it makes a spatial buffer of 15 km around the ground truth to discard any FALSE ALARMS outside this domain, the outcome of applying this analysis should give a revealing conclusion on the probability of detection of both algorithms.

There are several scoring methodologies that provide a better contrast between the two algorithms but are much more extense, this means that there is always going to be a compromise. Since we have a large ground truth database (tornados that are reported by ground surveys), for this particular report our compromise is quantity of experiments over quality of the result, we strongly believe that is more important to provide a specific statistical result for various cases, than several statistical results for few cases.

We must notice that in order for the experimentation to work, we must seek for cases in which both algorithms detected at least one time a tornadic event, the downside is that it will reduce the number of cases that will be actually used; this

will be done for every single tornado of a database of 376 tornados. We will be addressing this situation more clearly later in this report.

9.3 STUDY CASE EXAMPLE

Next we will study a case in order to get things in to perspective.

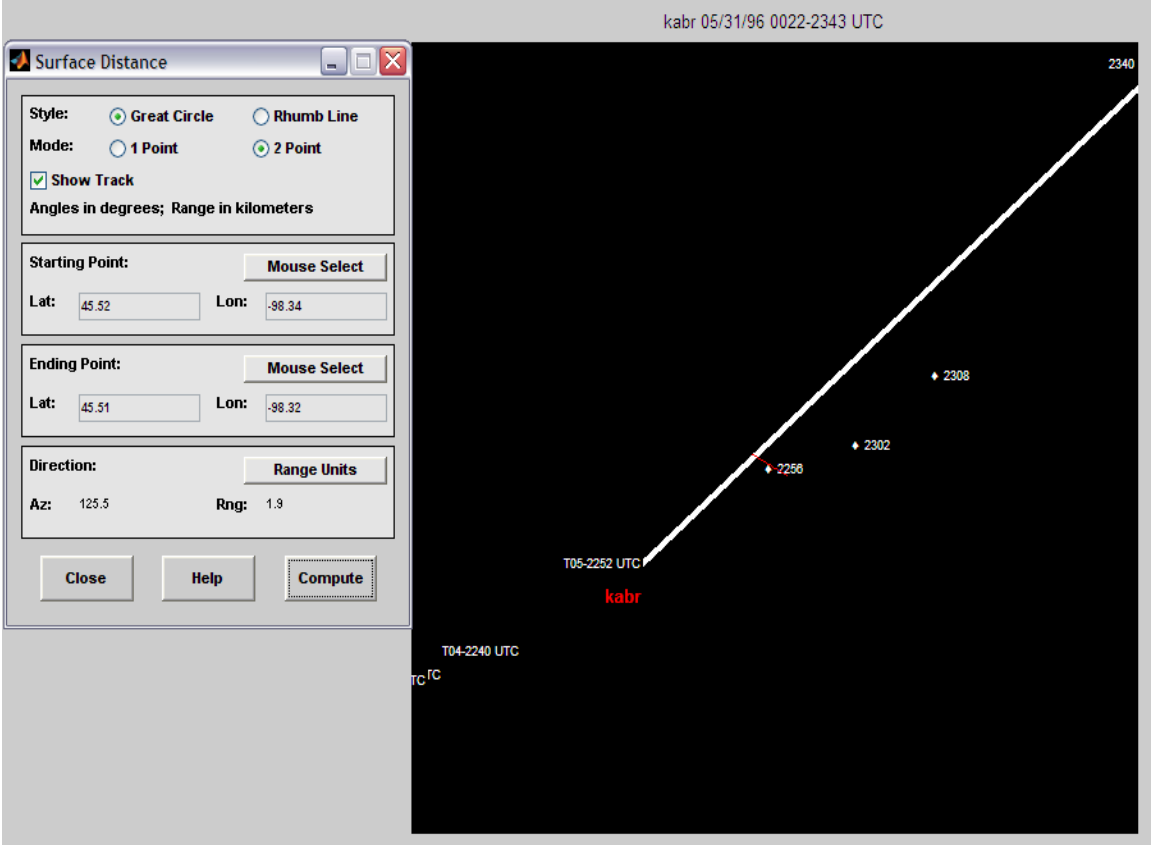

Figure 25. kabr 5/31/1996 T05, study case example, graphs provided by software developed by the author.

radar	date	tornado	time	F-Scale	Starting Range [Km]	path Width [m]	duration [min]	nftda	wdss2
kabr	5/31/1996	T05	2237	3	2	365.76	48	M	M
kabr	5/31/1996	T05	2242	3	2	365.76	48	M	M
kabr	5/31/1996	T05	2247	3	2	365.76	48	M	M
kabr	5/31/1996	T05	2252	3	2	365.76	48	M	M
kabr	5/31/1996	T05	2257	3	2	365.76	48	M	H
kabr	5/31/1996	T05	2302	3	2	365.76	48	M	H
kabr	5/31/1996	T05	2307	3	2	365.76	48	M	H
kabr	5/31/1996	T05	2312	3	2	365.76	48	M	M
kabr	5/31/1996	T05	2317	3	2	365.76	48	M	M
kabr	5/31/1996	T05	2322	3	2	365.76	48	M	M
kabr	5/31/1996	T05	2327	3	2	365.76	48	M	M

kabr	5/31/1996	T05	2332	3	2	365.76	48	M	M
kabr	5/31/1996	T05	2337	3	2	365.76	48	M	M
kabr	5/31/1996	T05	2342	3	2	365.76	48	M	M
kabr	5/31/1996	T05	2347	3	2	365.76	48	M	M

Table 5. FA=false alarm H=hit M=miss, c=null (no event and no detection), for study case example

In figure 25 we can see the ground truth data plotted as a white line with its respective label on the starting and ending point, the location of the radar in red and the results of the NSSL TDA as white rhombus with its respective time stamp. To the left of the graph we can see a tool used to calculate the distance between two user-specified points on the figure.

We can see that the NFTDA made no hits on the entire event, given that the tornado was strong, wide, close to radar and long in duration.

The results for this particular event where as follows:
From the definitions of POD, FAR, and CSI

$$POD = \frac{a}{a + c}$$

$$FAR = \frac{b}{a + b}$$

$$CSI = \frac{a}{a + b + c}$$

For NSSL TDA
a= 3;b=0; c=12 then POD=20% FAR=0% CSI=20%

For NFTDA
a=0; b=0; c=15 then POD=0% FAR =nan CSI=0%

This is a special case where there are no detections and false alarms for NFTDA; this will give an incorrect result in the FAR. For this reason this specific case is discarded this gives us a hint that we should be looking for cases in which both algorithms make a hit at least once or else we would be in the same situation.

10. STUDY CASES

10.1 KDDC DODGE CITY 2316 UTC 05/16/1995

We will start analyzing the first case that corresponds to kddc 05/16/95 Tornado label: T01.

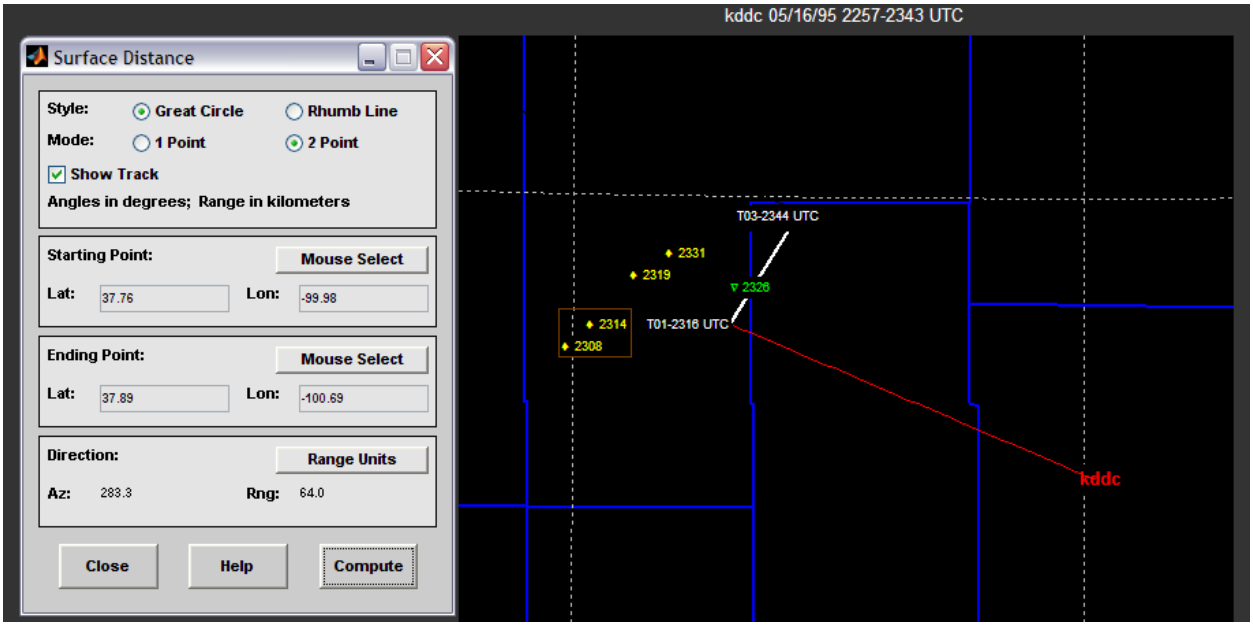

Figure 26. KDDC Dodge city, KS, 2316 UTC, distance from radar 82 km, EF scale 3, 731.52 m wide, graphs provided by software developed by the author.

Yellow nssl tda results, green nftda results, radar and distance to radar in red, in white ground truth data and starting and ending times.

We have explained before that we have to make a buffer of 15 km to count hits, misses and false alarms, inside this region. In figure 9 we can observe that two results from nssl tda (in brown), are outside of the 15 km buffer, so they will not be counted, also the tornado is moving north east relative to radar. The results are given in the following table.

radar	date	tornado	time	F-Scale	Starting Range [Km]	path Width [m]	duration [min]	nftda	wdss2

kddc	5/16/1995	T01	2300	3	82	731.5	19	M	M
kddc	5/16/1995	T01	2305	3	82	731.5	19	M	M
kddc	5/16/1995	T01	2310	3	82	731.5	19	M	M
kddc	5/16/1995	T01	2315	3	82	731.5	19	M	M
kddc	5/16/1995	T01	2320	3	82	731.5	19	M	H
kddc	5/16/1995	T01	2325	3	82	731.5	19	H	M
kddc	5/16/1995	T01	2330	3	82	731.5	19	M	H
kddc	5/16/1995	T01	2335	3	82	731.5	19	M	M
kddc	5/16/1995	T01	2340	3	82	731.5	19	M	M

Table 6. KDDC Dodge city, KS, 2316 UTC, results

FA= false alarm, H=hit, M=miss, o=nulls (no event and no detection).

For this case the score we have is:

POD NFTDA	FAR NFTDA	CSI NFTDA	POD NSSL	FAR NSSL	CSI NSSL
11.11	0	11.11	22.22	0	22.22

10.2 KDDC DODGE CITY 2135 UTC 05/26/1996

The next case we want to consider is:

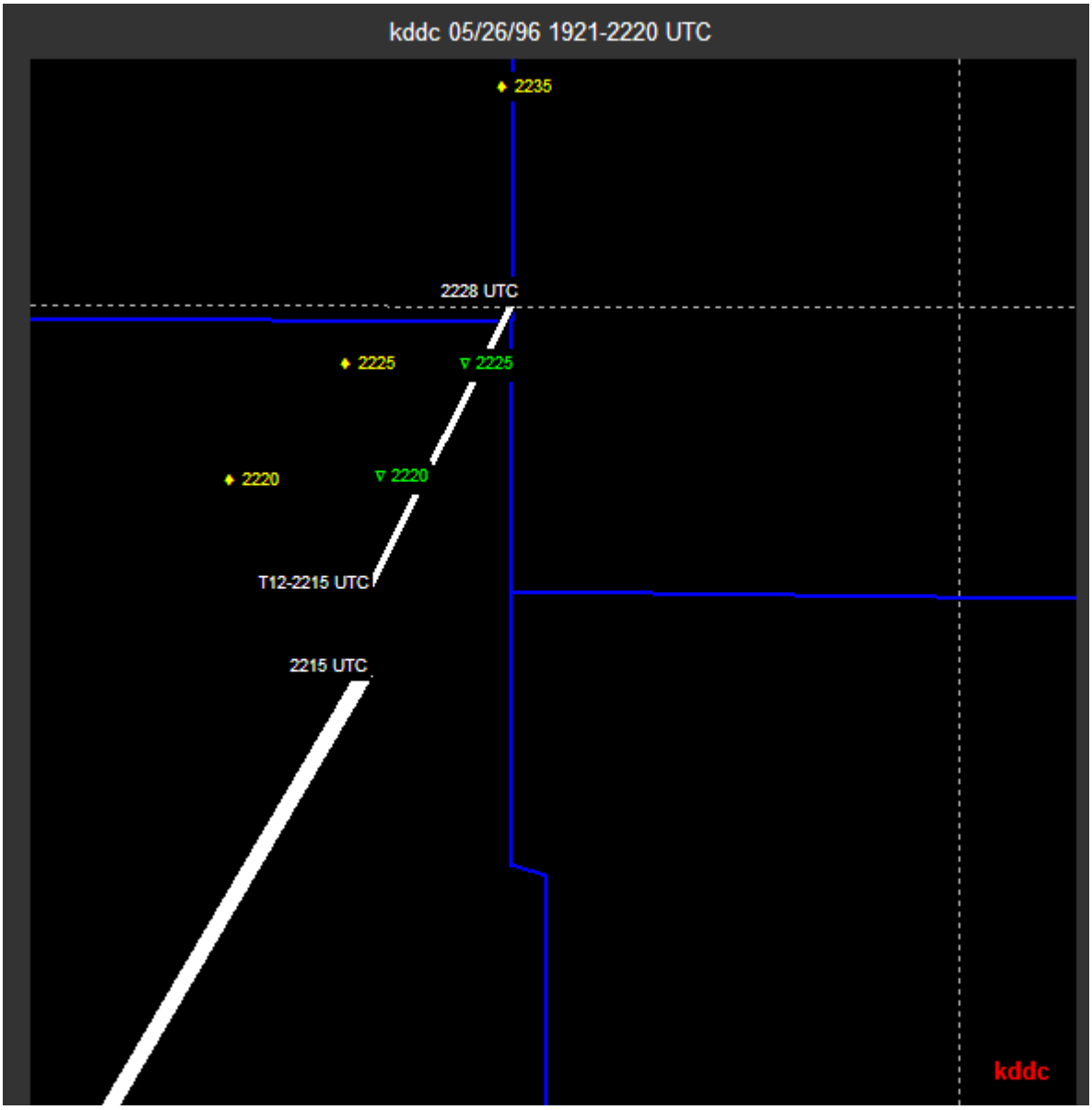

Figure 27. KDDC , Dodge city, KS, 2135 UTC, distance from radar 40 km, EF scale 1, 366 m wide, graphs provided by software developed by the author.

Yellow nssl tda results, green nftda results, radar and distance to radar in red, in white ground truth data and starting and ending times. Note that the tornado in

study is T12, and that there is another tornadic event finishing at 2215, that will not be studied, Tornado detections for this event were deleted for simplicity.

In figure 27 we can see T12 moving in North east direction with respect to radar,

radar	date	tornado	time	F-Scale	Starting Range [Km]	path Width [m]	duration [min]	nftda	wdss2
kddc	5/26/1996	T12	2200	1	40	366	13	M	M
kddc	5/26/1996	T12	2205	1	40	366	13	M	M
kddc	5/26/1996	T12	2210	1	40	366	13	M	M
kddc	5/26/1996	T12	2215	1	40	366	13	M	M
kddc	5/26/1996	T12	2220	1	40	366	13	H	H
kddc	5/26/1996	T12	2225	1	40	366	13	H	H
kddc	5/26/1996	T12	2230	1	40	366	13	M	M

Table 7. Results for KDDC dodge city 2135 UTC 05/26/1996

this tornado is closer than the first example, yet, it more narrow and has a shorter life span. The results for this event are given in table 7.

The scoring results are given next:

POD NFTDA	FAR NFTDA	CSI NFTDA	POD NSSL	FAR NSSL	CSI NSSL
25	0	25	37.5	0	37.5

10.3 KENX ALBANY NY 2019 UTC 05/31/1998

The next case in our study is:

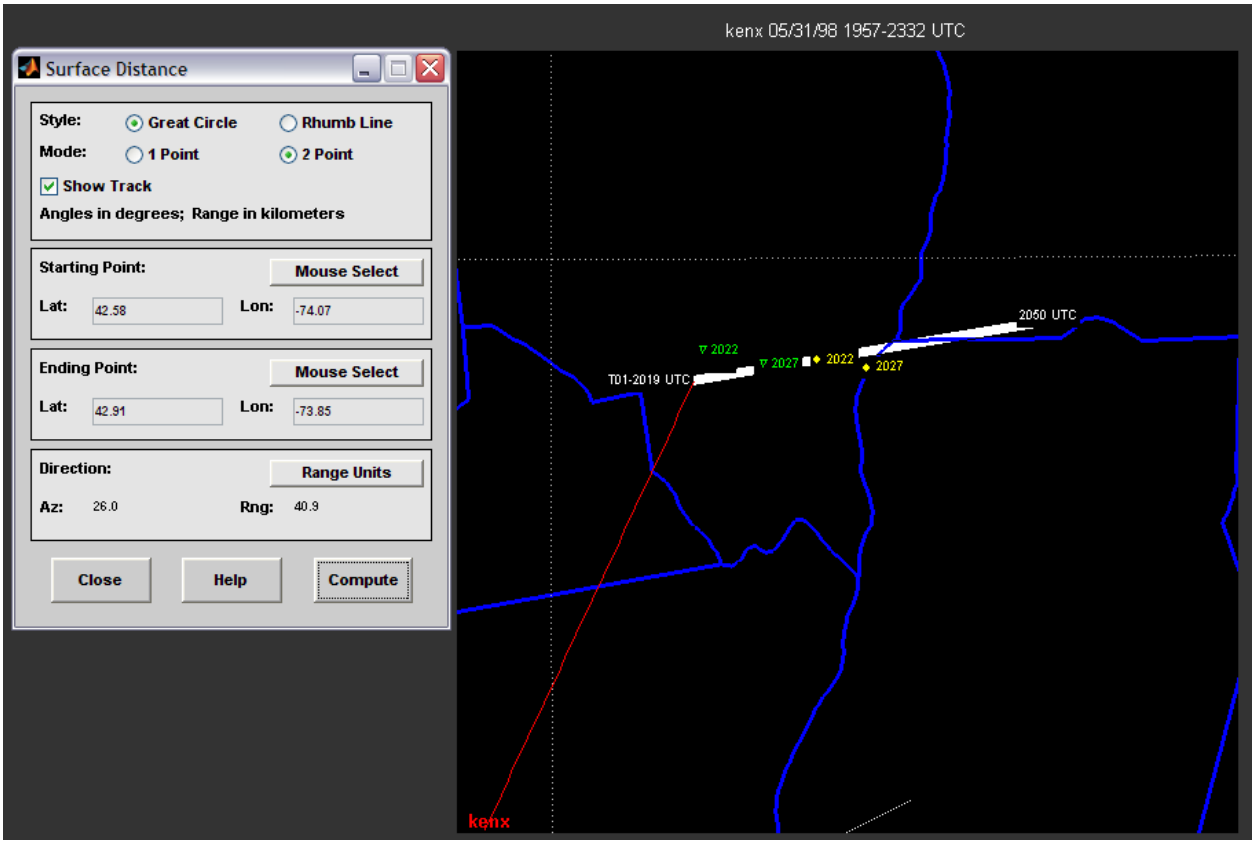

Figure 28. KENX, Albany, NY 2019 UTC, distance from radar 43 km, EF scale 3, 887 m wide., graphs provided by software developed by the author.

Yellow nssl tda results, green nftda results, radar and distance to radar in red, in white ground truth data and starting and ending times. Other detections are erased according to 15 km buffer.

For this case kenx 05/31/98 T01, we have again a relatively close tornado with EF scale 3 and relatively wide. We erased detections according to 15 km buffer proposed in the scoring methodology, this can be helpful for cases in which many tornados occur, in that way false alarms or hits from other locations wont bias the studied case. Table 8 shows the results,

radar	date	tornado	time	F-Scale	Starting Range [Km]	path Width [m]	duration [min]	nftda	wdss2
kenx	5/31/1998	T01	2005	3	43	887	31	M	M
kenx	5/31/1998	T01	2010	3	43	887	31	M	M
kenx	5/31/1998	T01	2015	3	43	887	31	M	M
kenx	5/31/1998	T01	2020	3	43	887	31	H	H
kenx	5/31/1998	T01	2025	3	43	887	31	H	H
kenx	5/31/1998	T01	2030	3	43	887	31	M	M
kenx	5/31/1998	T01	2035	3	43	887	31	M	M
kenx	5/31/1998	T01	2040	3	43	887	31	M	M
kenx	5/31/1998	T01	2045	3	43	887	31	M	M
kenx	5/31/1998	T01	2050	3	43	887	31	M	M
kenx	5/31/1998	T01	2055	3	43	887	31	M	M

Table 8. Results for KENX Albany NY 2019 UTC 05/31/1998

The scoring goes as follows:

POD NFTDA	FAR NFTDA	CSI NFTDA	POD NSSL	FAR NSSL	CSI NSSL
18.18	0	18.18	18.18	0	18.18

10.4 KENX ALBANY NY 2130 UTC 05/31/1998

The next case we would like to present is

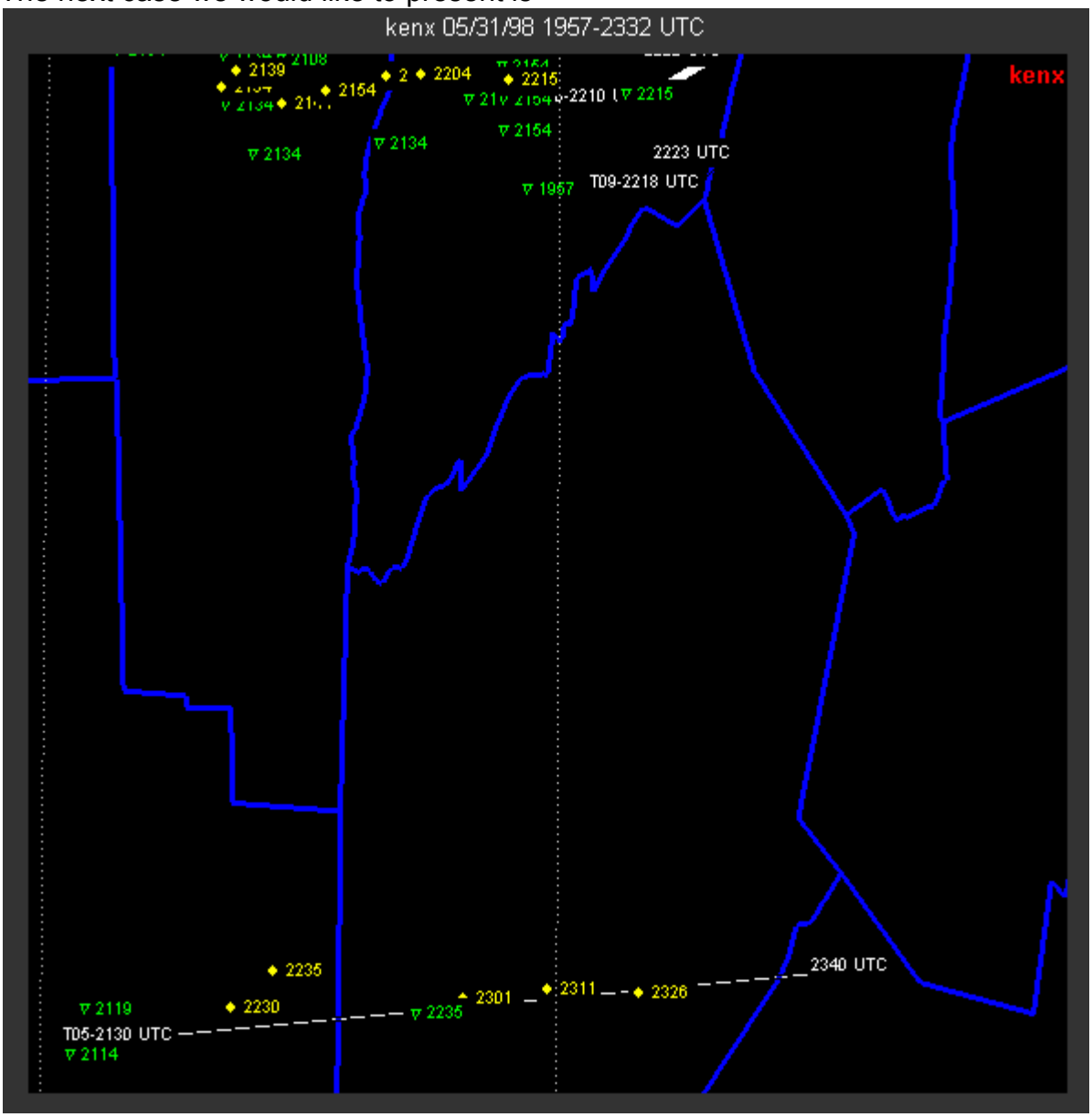

Figure 29. KENX, Albany, NY 2130 UTC, distance from radar 195 km, EF scale 3, 183 m wide, graphs provided by software developed by the author.

Yellow nssl tda results, green nftda results, radar and distance to radar in red, in white ground truth data and starting and ending times. Other detections are erased according to 15 km buffer.

In figure 29, we will select T05 for our study, which evolves, south east. In this case we can see detections from nssl tda and nftda at a far range, both algorithms correctly identified the tornado at some point, even though it was at a considerable distance from radar, this tornado is characterized for having a long life span.. Let's see what are the results (table 9), notice there is a false alarm on 2114 UTC from nftda. We will not study this false alarm in detail since its only due to timing, since its right on top of ground truth.

radar	date	tornado	time	F-Scale	Starting Range [Km]	path Width [m]	duration [min]	nftda	wdss2
kenx	5/31/1998	T05	2114	3	195	182	130	FA	o
kenx	5/31/1998	T05	2115	3	195	182	130	M	M
kenx	5/31/1998	T05	2120	3	195	182	130	H	M
kenx	5/31/1998	T05	2125	3	195	182	130	M	M
kenx	5/31/1998	T05	2135	3	195	182	130	M	M
kenx	5/31/1998	T05	2140	3	195	182	130	M	M
kenx	5/31/1998	T05	2145	3	195	182	130	M	M
kenx	5/31/1998	T05	2150	3	195	182	130	M	M
kenx	5/31/1998	T05	2155	3	195	182	130	M	M
kenx	5/31/1998	T05	2200	3	195	182	130	M	M
kenx	5/31/1998	T05	2205	3	195	182	130	M	M
kenx	5/31/1998	T05	2210	3	195	182	130	M	M
kenx	5/31/1998	T05	2215	3	195	182	130	M	M
kenx	5/31/1998	T05	2220	3	195	182	130	M	M
kenx	5/31/1998	T05	2225	3	195	182	130	M	M
kenx	5/31/1998	T05	2230	3	195	182	130	M	H
kenx	5/31/1998	T05	2235	3	195	182	130	H	H
kenx	5/31/1998	T05	2240	3	195	182	130	M	M
kenx	5/31/1998	T05	2245	3	195	182	130	M	M
kenx	5/31/1998	T05	2250	3	195	182	130	M	M
kenx	5/31/1998	T05	2255	3	195	182	130	M	M
kenx	5/31/1998	T05	2300	3	195	182	130	M	H
kenx	5/31/1998	T05	2305	3	195	182	130	M	M
kenx	5/31/1998	T05	2310	3	195	182	130	M	H
kenx	5/31/1998	T05	2315	3	195	182	130	M	M
kenx	5/31/1998	T05	2320	3	195	182	130	M	M
kenx	5/31/1998	T05	2325	3	195	182	130	M	H

kenx	5/31/1998	T05	2330	3	195	182	130	M	M
kenx	5/31/1998	T05	2335	3	195	182	130	M	M
kenx	5/31/1998	T05	2340	3	195	182	130	M	M
kenx	5/31/1998	T05	2345	3	195	182	130	M	M

Table 9. Results for KENX, Albany, NY 2130 UTC, distance from radar 195 km, EF scale 3, 183 m wide

The scores are as follows:

POD NFTDA	FAR NFTDA	CSI NFTDA	POD NSSL	FAR NSSL	CSI NSSL
6.66	33.33	6.45	16.66	0	16.66

10.5 KFSD SIOUX FALLS SD 2155 UTC 03/29/1998

The next case we would like to propose is:

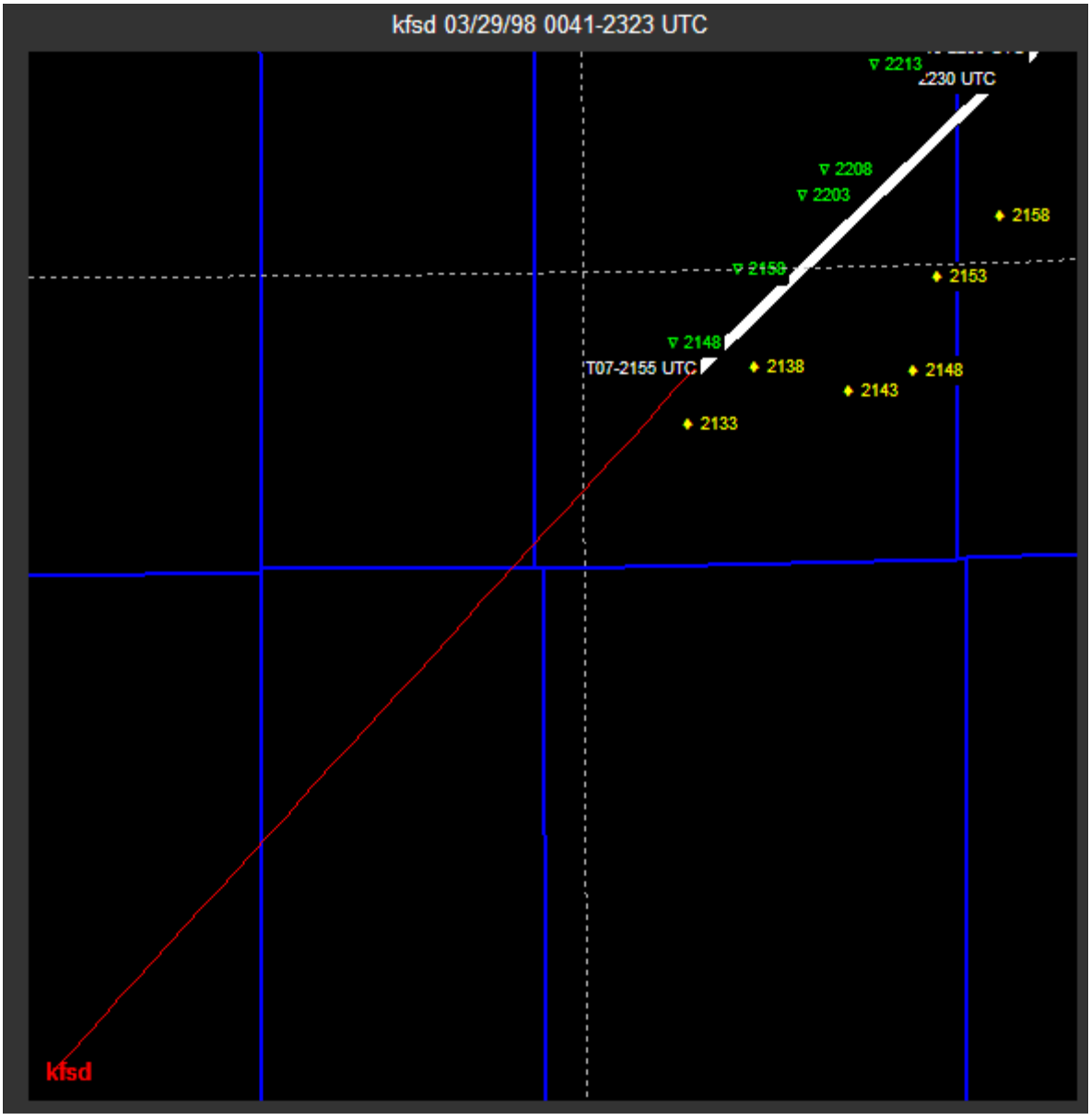

Figure 30. KFSD Sioux Falls, SD 2155 UTC, distance from radar 107 km, EF scale 3, 823 m, graphs provided by software developed by the author.

Yellow nssl tda results, green nftda results, radar and distance to radar in red, in white ground truth data and starting and ending times. Other detections and

tornadoes are erased according to 15 km buffer and event under study, respectively.

In figure 30 we can see T07 marked from kfsd radar, in red. This tornado is characterized by its distance (107 km) from radar and its relatively long life span. In table 10 we can see the results.

radar	date	tornado	time	F-Scale	Starting Range [Km]	path Width [m]	duration [min]	nftda	wdss2
kfsd	3/29/1998	T07	2133	3	107	823	35	o	FA
kfsd	3/29/1998	T07	2138	3	107	823	35	o	FA
kfsd	3/29/1998	T07	2140	3	107	823	35	M	M
kfsd	3/29/1998	T07	2145	3	107	823	35	M	H
kfsd	3/29/1998	T07	2150	3	107	823	35	H	H
kfsd	3/29/1998	T07	2155	3	107	823	35	M	H
kfsd	3/29/1998	T07	2200	3	107	823	35	H	H
kfsd	3/29/1998	T07	2205	3	107	823	35	H	M
kfsd	3/29/1998	T07	2210	3	107	823	35	H	M
kfsd	3/29/1998	T07	2215	3	107	823	35	H	M
kfsd	3/29/1998	T07	2220	3	107	823	35	M	M
kfsd	3/29/1998	T07	2225	3	107	823	35	M	M
kfsd	3/29/1998	T07	2230	3	107	823	35	M	M
kfsd	3/29/1998	T07	2235	3	107	823	35	M	M

Table 10. Results for kfsd sioux falls, SD 2155 UTC 03/29/1998

The score reflects the first time the nftda is superior, according to this methodology.

POD NFTDA	FAR NFTDA	CSI NFTDA	POD NSSL	FAR NSSL	CSI NSSL
41.66	0	41.66	33.33	33.33	28.57

10.6 KFWS DALLAS FORTH WORTH TX 2155 UTC 03/29/1998

The next case we would like to propose is:

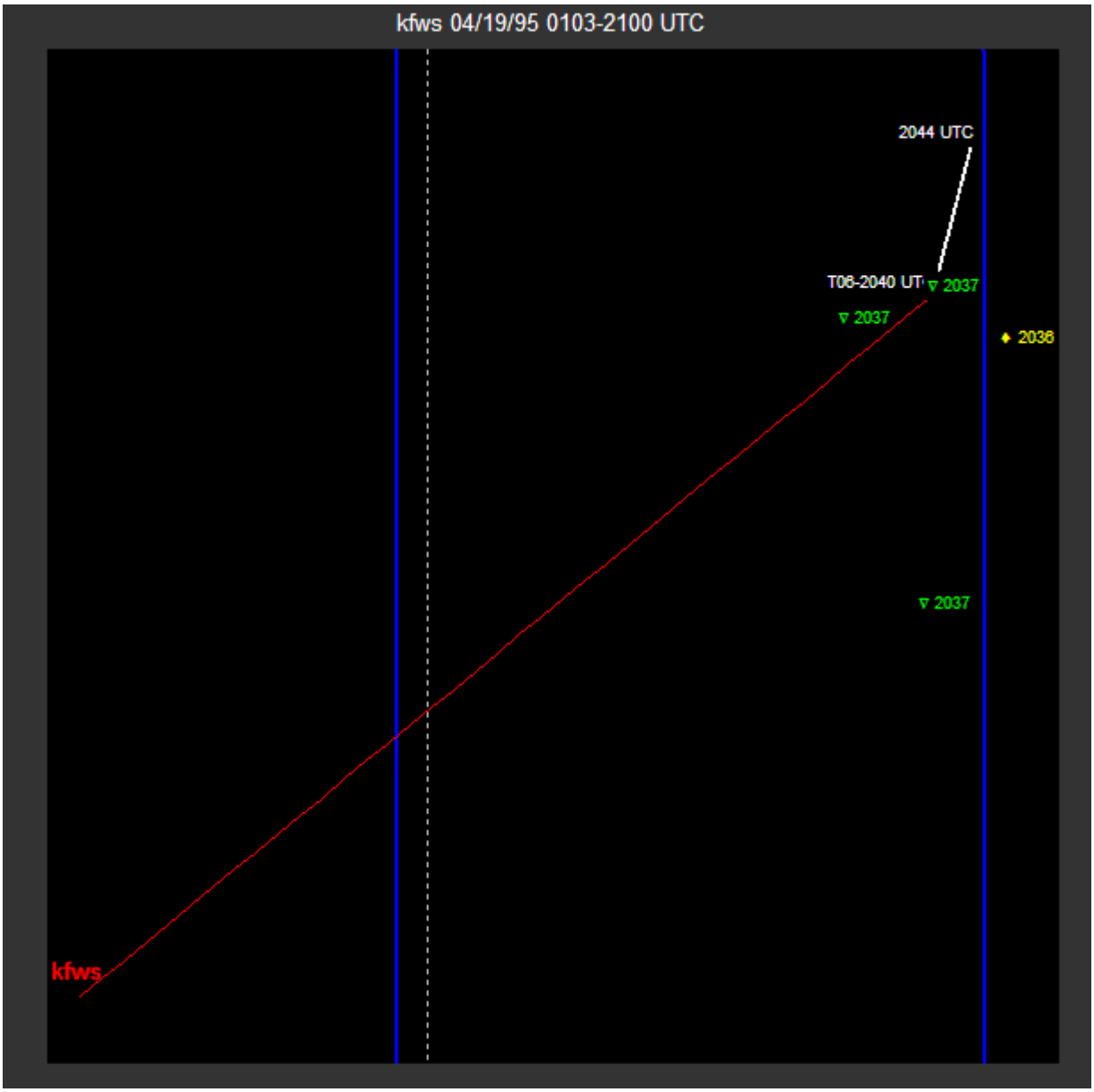

Figure 31. KFWS Dallas Forth Worth, TX 2155 UTC, distance from radar 83 km, EF scale 1, and 91.44 m wide, graphs provided by software developed by the author.

Yellow nssl tda results, green nftda results, radar and distance to radar in red, in white ground truth data and starting and ending times. Other detections and

tornadoes are erased according to 15 km buffer and event under study, respectively.
For figure 31, notice there is detection from NFTDA that is approximately 4 km away from ground truth; we will first study this in order to provide a better perspective on the nature of the algorithm. We also notice the tornado is weak and far.

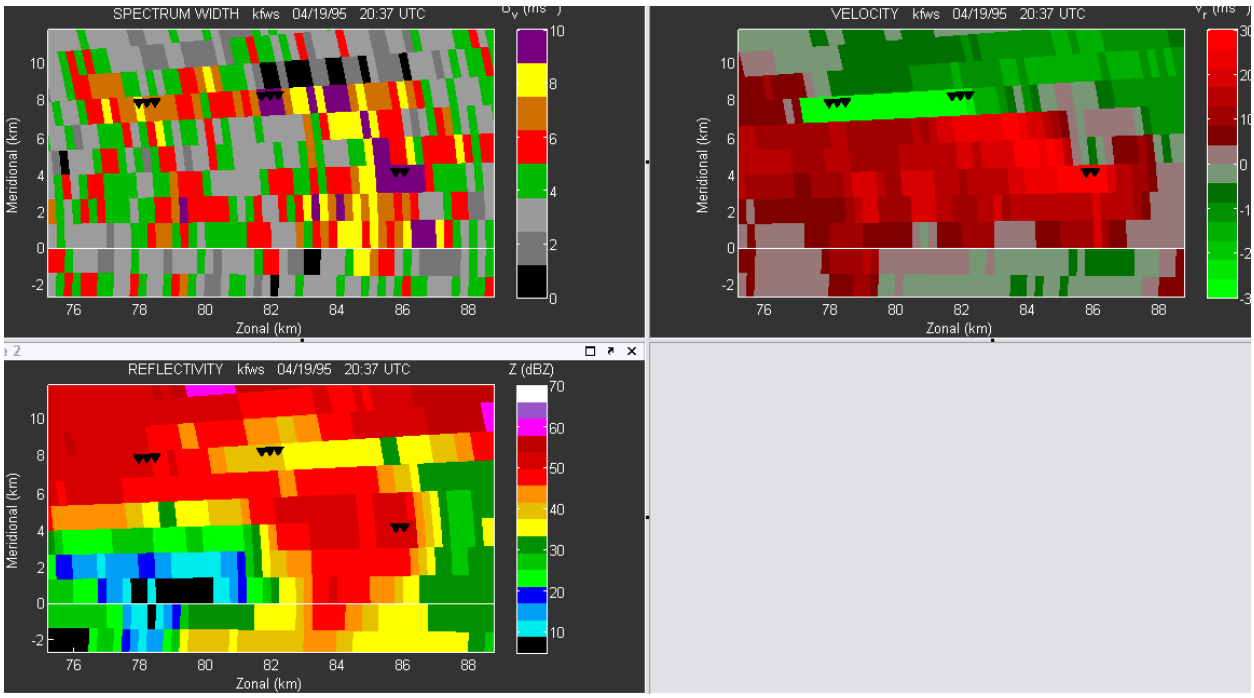

Figure 32. KFWS 04/19/1995 2037 UTC, from top left to bottom right, Spectrum width, velocity and reflectivity plots, graphs provided by software developed by the author.

Notice there is a detection separated 4 km in the meridional plane from the other two.

Figure 32 shows roughly the conditions for which the nftda issues detections; we see high reflectivity values, accompanied by strong azimuthal shear, and wide spectrum. This indicates that we should use the additional input parameters the nftda posses in order to obtain better detection results (previously discussed in nftda overview chapter). Even though these parameters characterize better a tornadic event, the utilization of these is beyond scope of this report.
Results are shown in table 11.

radar	date	tornado	time	F-Scale	Starting Range [Km]	path Width [m]	duration [min]	nftda	wdss2	
kfws	4/19/1995	T06	2025	1	83	91.44	4	M	M	
kfws	4/19/1995	T06	2030	1	83	91.44	4	M	M	
kfws	4/19/1995	T06	2035	1	83	91.44	4	H	H	
kfws	4/19/1995	T06	2040	1	83	91.44	4	M	M	
kfws	4/19/1995	T06	2045	1	83	91.44	4	M	M	
Kfws	4/19/1995	T06	2050	1	83	91.44	4	M	M	

Table 11. Results for KFWS 04/19/1995 2037 UTC, from top left to bottom right, Spectrum width, velocity and reflectivity plots

POD NFTDA	FAR NFTDA	CSI NFTDA	POD NSSL	FAR NSSL	CSI NSSL
16.66	0	16.66	16.66	0	16.66

10.7 KFWS DALLAS FORTH WORTH TX 2053 UTC 05/07/1995

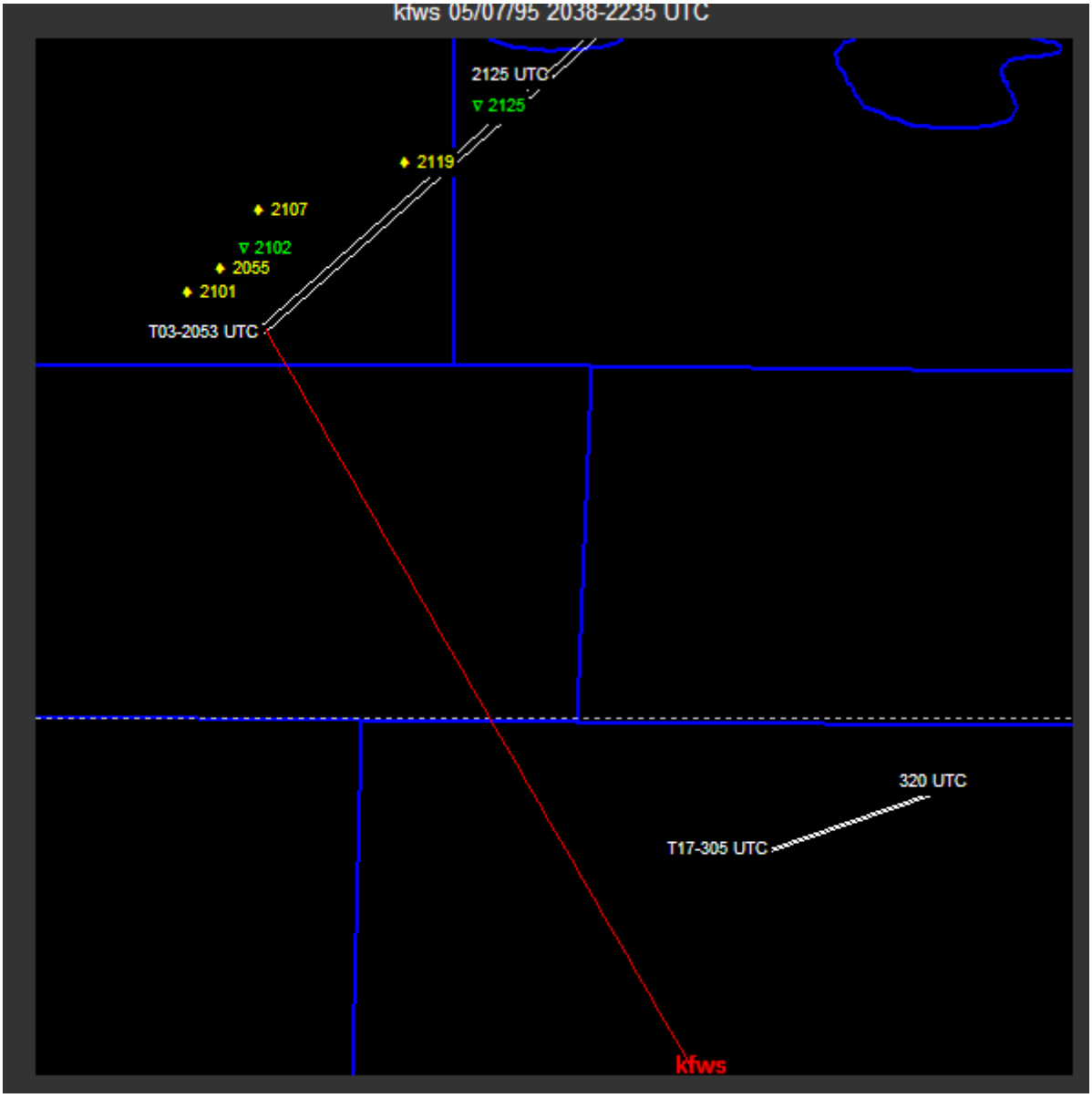

Figure 33. KFWS Dallas Forth Worth, TX 2053 UTC, distance from radar 106 km, EF scale 3, and 804 m wide., graphs provided by software developed by the author.

Yellow nssl tda results, green nftda results, radar and distance to radar in red, in white ground truth data and starting and ending times. Other detections and tornadoes are erased according to 15 km buffer and event under study, respectively.

This is another tornado with same characteristics as some before, relatively far, EF scale 3, with 804 in width. Results are given in the following 2 table

radar	date	tornado	time	F-Scale	Starting Range [Km]	path Width [m]	duration [min]	nftda	wdss2
kfws	5/7/1995	T03	2040	3	106	804	34	M	M
kfws	5/7/1995	T03	2045	3	106	804	34	M	M
kfws	5/7/1995	T03	2050	3	106	804	34	M	M
kfws	5/7/1995	T03	2055	3	106	804	34	M	H
kfws	5/7/1995	T03	2100	3	106	804	34	H	H
kfws	5/7/1995	T03	2105	3	106	804	34	M	H
kfws	5/7/1995	T03	2110	3	106	804	34	M	M
kfws	5/7/1995	T03	2115	3	106	804	34	M	M
kfws	5/7/1995	T03	2120	3	106	804	34	M	H
kfws	5/7/1995	T03	2125	3	106	804	34	H	M
kfws	5/7/1995	T03	2130	3	106	804	34	M	M

Table 12. KFWS Dallas Forth Worth, TX 2053 UTC.

POD NFTDA	FAR NFTDA	CSI NFTDA	POD NSSL	FAR NSSL	CSI NSSL
18.18	0	18.18	30	0	30

10.8 KGLD GOODLAND KS 2015 UTC 05/12/1995

Next we will study a case in which 3 important tornadoes have developed,

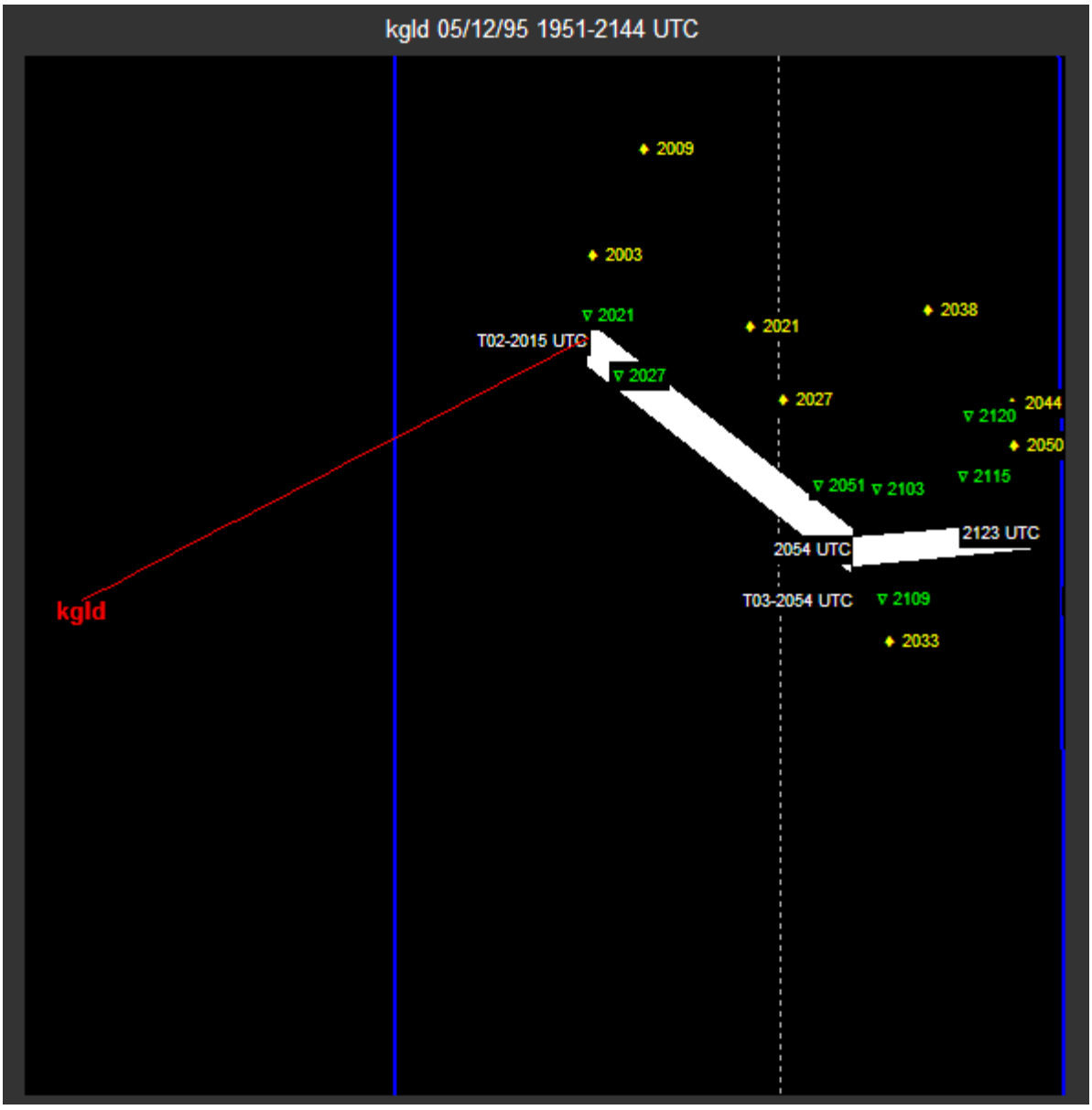

Figure 34. KGLD Goodland, KS, T02 2015 UTC, distance from radar 57 km, EF scale 2, and 1.73 Km wide, T03 2054 UTC, 86 Km from radar, Ef scale 2 and 914.4 m wide, **graphs provided by software developed by the author.**

Yellow nssl tda results, green nftda results, radar and distance to radar in red, in white ground truth data and starting and ending times. Other detections and

tornadoes are erased according to 15 km buffer and event under study, respectively.

We are going to observe three different tornadoes developed near Colby county on KS, the T02, T03 and T04, this tornadoes are characterized by its width, they are at 57, 86 and 123 km from radar respectively, with a EF scale of 2, usually this could be hard to locate with radar, but once again, nftda shows it has better accuracy than nssl tda, nevertheless nssl tda has shown a better overall performance so far, let see the results which are depicted in table 13.

To have a better view we can use figure 18.

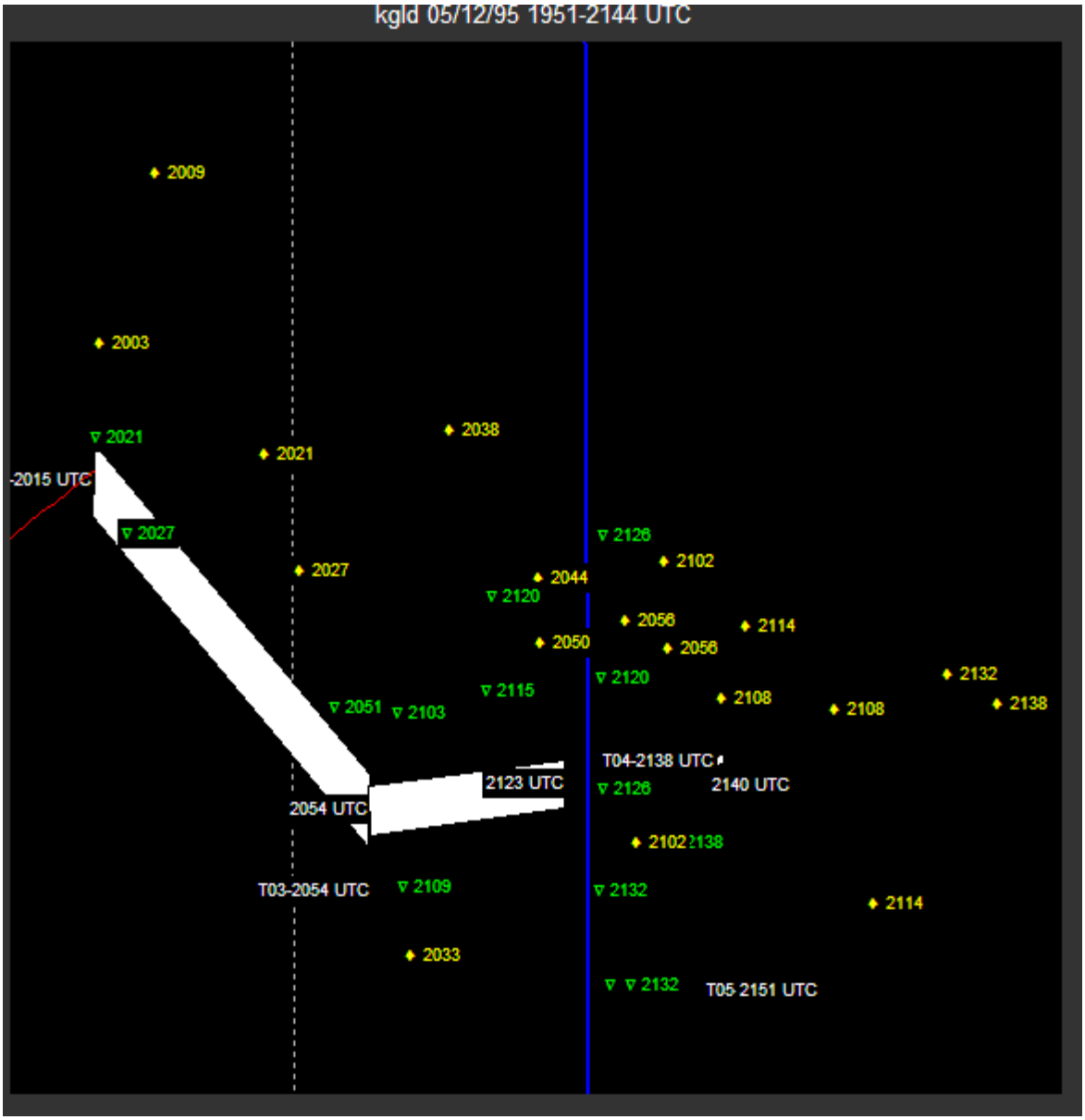

Figure 35. zoomed in view for KGLD GOOLAND 2015 UTC AND 2054 UTC, graphs provided by software developed by the author.

radar	date	tornado	time	F-Scale	Starting Range [Km]	path Width [m]	duration [min]	nftda	wdss2
kgld	5/12/1995	T02	2000	2	57	1372	39	M	M
kgld	5/12/1995	T02	2005	2	57	1372	39	M	H
kgld	5/12/1995	T02	2010	2	57	1372	39	M	H
kgld	5/12/1995	T02	2015	2	57	1372	39	M	M
kgld	5/12/1995	T02	2020	2	57	1372	39	H	H
kgld	5/12/1995	T02	2025	2	57	1372	39	H	H

kgld	5/12/1995	T02	2030	2	57	1372	39	M	M
kgld	5/12/1995	T02	2035	2	57	1372	39	M	H
kgld	5/12/1995	T02	2040	2	57	1372	39	M	H
kgld	5/12/1995	T02	2045	2	57	1372	39	M	H
kgld	5/12/1995	T02	2050	2	57	1372	39	H	H
kgld	5/12/1995	T02	2055	2	57	1372	39	M	H
kgld	5/12/1995	T02	2100	2	57	1372	39	M	H
kgld	5/12/1995	T03	2040	2	86	914	39	M	M
kgld	5/12/1995	T03	2045	2	86	914	39	M	M
kgld	5/12/1995	T03	2050	2	86	914	39	M	M
kgld	5/12/1995	T03	2055	2	86	914	39	M	M
kgld	5/12/1995	T03	2100	2	86	914	39	M	H
kgld	5/12/1995	T03	2105	2	86	914	39	H	M
kgld	5/12/1995	T03	2110	2	86	914	39	H	H
kgld	5/12/1995	T03	2115	2	86	914	39	H	H
kgld	5/12/1995	T03	2120	2	86	914	39	H	M
kgld	5/12/1995	T03	2125	2	86	914	39	M	M
kgld	5/12/1995	T04	2125	2	123	182	2	H	M
kgld	5/12/1995	T04	2130	2	123	182	2	H	H
kgld	5/12/1995	T04	2135	2	123	182	2	H	H
kgld	5/12/1995	T04	2140	2	123	182	2	M	M
kgld	5/12/1995	T04	2145	2	123	182	2	M	M

POD NFTDA	FAR NFTDA	CSI NFTDA	POD NSSL	FAR NSSL	CSI NSSL
23.07	0	23.07	76.92	0	76.92
33.33	0	33.33	30	0	30
60	0	60	40	0	40

Table 13. Results for KGLD goodland KS 2015 UTC 05/12/1995

We can see the slight difference in results between the two algorithms; nftda is still having much better location accuracy than nssl tda

10.9 KJAN JACKSON MISSISSIPPI 0910 UTC 11/11/1995

The next case in our study is:

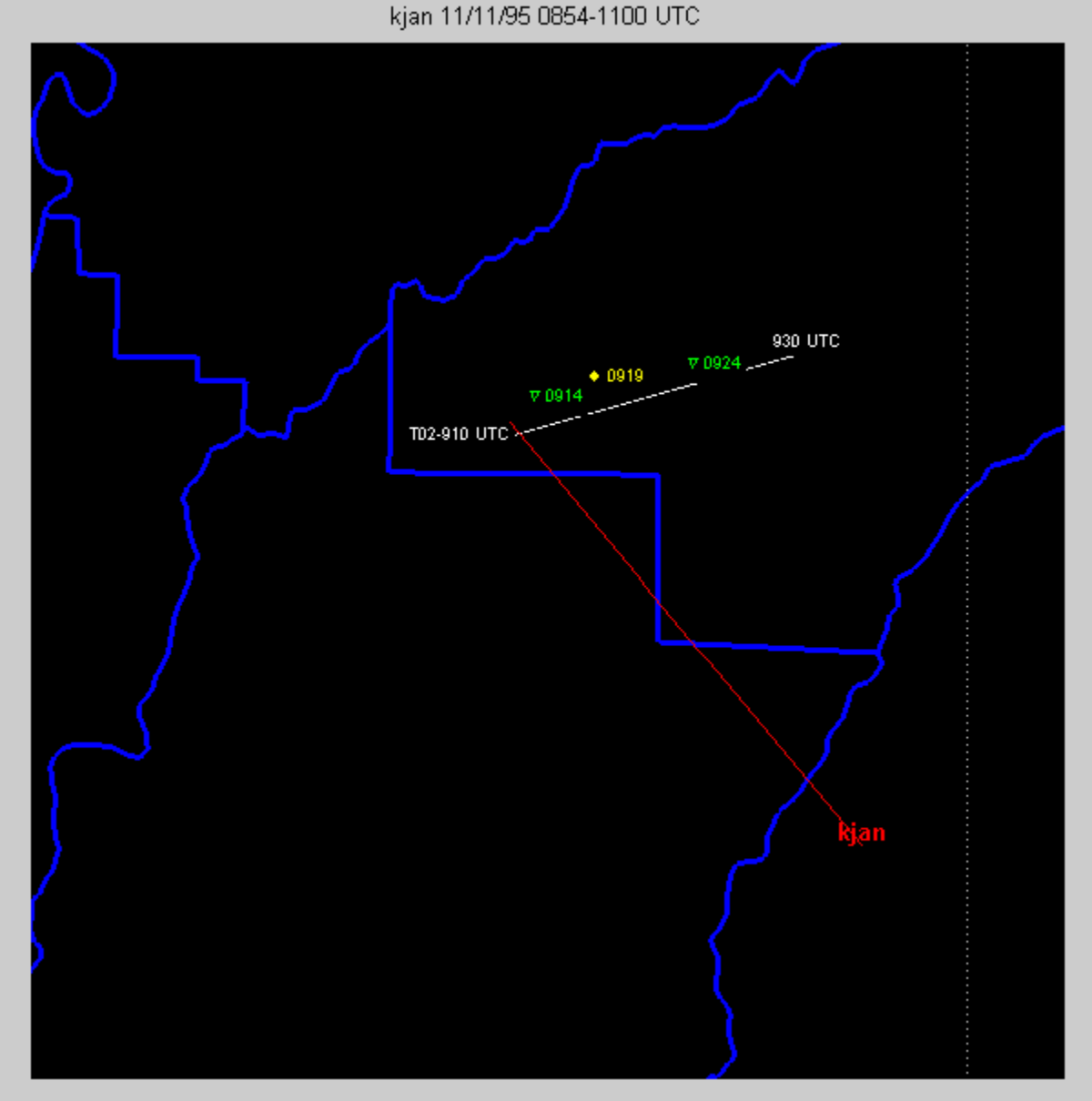

Figure 36. KJAN Jackson, Mississippi T02 0910 UTC, distance from radar 37 km, EF scale 3, and 183 m wide., graphs provided by software developed by the author.

Yellow nssl tda results, green nftda results, radar and distance to radar in red, in white ground truth data and starting and ending times. Other detections and tornadoes are erased according to 15 km buffer and event under study, respectively.

The results are shown in the next tables,

radar	date	tornado	time	F-Scale	Starting Range [Km]	path Width [m]	duration [min]	nftda	wdss2
kjan	11/11/1995	T02	855	3	37	183	20	M	M
kjan	11/11/1995	T02	900	3	37	183	20	M	M
kjan	11/11/1995	T02	905	3	37	183	20	M	M
kjan	11/11/1995	T02	910	3	37	183	20	M	M
kjan	11/11/1995	T02	915	3	37	183	20	H	M
kjan	11/11/1995	T02	920	3	37	183	20	M	H
kjan	11/11/1995	T02	925	3	37	183	20	H	M
kjan	11/11/1995	T02	930	3	37	183	20	M	M
kjan	11/11/1995	T02	935	3	37	183	20	M	M

Table 14. Results for KJAN Jackson Mississippi 0910 UTC 11/11/1995

The scoring table is as follows:

POD NFTDA	FAR NFTDA	CSI NFTDA	POD NSSL	FAR NSSL	CSI NSSL
22.22	0	22.22	11.11	0	11.11

11. OVERALL SCORING RESULTS

The result of the scoring is shown in table 15.

POD NFTDA	FAR NFTDA	CSI NFTDA	POD NSSL	FAR NSSL	CSI NSSL
25.0972727	33.33	25.0781818	30.2345455	33.33	29.8018182

The results are evident; the NSSL TDA performs better under the scoring proposed in this report, There are some issues we want to address, first, the NFTDA algorithm currently tested had simple threshold on range and reflectivity values, that can be a problem, since some of the tornadoes can also be detected very near the radar. Second, the algorithm lacks of an accurate suppression of range and azimuth continuity, in that way the NFTDA sometimes detected mesocyclones which did not formed into tornadoes. Third, we must notice that we only used 2 of the 5 parameters that are actually employed by the original NFTDA, performance under this conditions must be subject to further review after assessing a final conclusion.

Overall the NFTDA algorithm behaved better than the NSSL TDA in most of the cases, detecting the tornados (location-wise) more accurately, this proves that even with 2 of its 5 parameters, and some adjustments in the algorithm it can be properly set to function even better than NSSL TDA.

12. CONCLUSIONS

This report is yet to be concluded entirely, it has been talked previously that the scoring methodology was not optimal, but instead it gives an overall result, which is valid. There are two major disadvantages of using the current scoring methodology which are:

- Not all the samples from a complete day where included in the calculation of the NSSL TDA OR NFTDA, it means, that there was a possibility of some False alarms that was not accounted for in the scoring. The selection of netcdf files that were used to obtain the NSSL TDA and NFTDA was made according to a complete buffer of -15+ti_day_first tornado and tf_day_last tornado +5; ie. If the first tornado of the day (studied case) occurred at 02:00 UTC and the last tornado of the day finished at 5:00 UTC, then the data selected to apply NSSL TDA and NFTDA was 1:45 UTC to 5:05 UTC, because of this some false alarms that might have occurred at, ie 01:00 UTC where not accounted for.

-The buffer of 15 Km might have been excessive?, this opens the discussion on False alarms also, since some false alarms that occurred at ranges greater than 15 Km where not accounted for. This buffer could be made smaller, and the the POD will decrease (in theory, not necessarily true for all cases), and it could be wider, and the POD will in theory increase (not necessarily true for all cases).

There are some concerns we want to discuss regarding algorithm structure (for the Reflectivity, Spectrum width and Velocity difference),

-First, the NFTDA algorithm currently tested had simple threshold on range and reflectivity values, that can be a problem, since some of the tornadoes can also be detected very near the radar.

-Second, the algorithm lacks of an accurate suppression of range and azimuth continuity, since there were some detections where large non tornadic events where present.

-Third, we must notice that we only used 2 of the 5 parameters that are actually employed by the original NFTDA, performance under this conditions must be subject to further review after assessing a final conclusion.

Overall the NFTDA algorithm behaved better than the NSSL TDA in most of the cases, detecting the tornados (location-wise) more accurately, this proves that even with 2 of its 5 parameters, and some adjustments in the algorithm it can be properly set to function even better than NSSL TDA

13. REFERENCES

Brown, R.A., 1998: Nomogram for Aiding the Interpretation of Tornadic Vortex Signatures Measured by Doppler Radar. *Wea. Forecasting*, **13**, 505–512.

Crum, T.D., and R.L. Alberty, 1993: The WSR-88D and the WSR-88D Operational Support Facility. *Bull. Amer. Meteor. Soc.*, **74**, 1669–1687.

Doviak, R. J., and D. S. Zrnic, 1993: *Doppler Radar and Weather Observations*. 2d ed. Academic Press, 562 pp.

Marzban, C., and G.J. Stumpf, 1996: A Neural Network for Tornado Prediction Based on Doppler Radar-Derived Attributes. *J. Appl. Meteor.*, **35**, 617–626.

Merrill I. Skolnik: Introduction to Radar Systems. Format: Textbook Hardcover, 672pp Publisher: McGraw-Hill Higher Education Pub. Date: December 2002.

Merrill I. Skolnik .Radar Handbook. Format: Hardcover, 1328pp. Publisher: McGraw-Hill Professional Publishing .Pub. Date: February 2008

Mitchell, E.D., S.V. Vasiloff, G.J. Stumpf, A. Witt, M.D. Eilts, J.T. Johnson, and K.W. Thomas, 1998: The National Severe Storms Laboratory Tornado Detection Algorithm. *Wea. Forecasting*, **13**, 352–366.

Smith, R.L., And D.W. Holmes, 1961: Use Of Doppler Radar In Meteorological Observations. *Mon. Wea. Rev.*, **89**, 1–7.

Tian-You Yu, University of Oklahoma, Norman, OK; and A. Shapiro, D. S. Zrnic, M. P. Foster, D. L. Andra, Jr., R. J. Doviak, and M. B. Yeary-2004

Tipton, G.A., E.D. Howieson, J.A. Margraf, and R.R. Lee, 1998: Optimizing the WSR-88D Mesocyclone/Tornadic Vortex Signature Algorithm Using WATADS—A Case Study*. *Wea. Forecasting*, **13**, 367–376.
Whiton, R.C., P.L. Smith, S.G. Bigler, K.E. Wilk, and A.C. Harbuck, 1998: History of Operational Use of Weather Radar by U.S. Weather Services. Part I: The Pre-NEXRAD Era. *Wea. Forecasting*, **13**, 219–243.

Whiton, R.C., P.L. Smith, S.G. Bigler, K.E. Wilk, and A.C. Harbuck, 1998: History of Operational Use of Weather Radar by U.S. Weather Services. Part II: Development of Operational Doppler Weather Radars. *Wea. Forecasting*, **13**, 244–252.

Wilks,D.S.,1995: Statistical Methods in the Atmospheric Sciences.AcademicPress,467pp.

Witt, A., M.D. Eilts, G.J. Stumpf, E.D. Mitchell, J.T. Johnson, and K.W. Thomas, 1998: Evaluating the Performance of WSR-88D Severe Storm Detection Algorithms. *Wea. Forecasting*, **13**, 513–518.